Robotica (2016) volume 34, pp. 2415–2439. © Cambridge University Press 2015
doi:10.1017/S0263574715000090

# Angularity and axiality of a Schönflies parallel manipulator

J. Jesús Cervantes-Sánchez*, José M. Rico-Martínez and Víctor H. Pérez-Muñoz

*Universidad de Guanajuato, DICIS, Departamento de Ingeniería Mecánica 36885, Salamanca, Guanajuato, México.*
*E-mails: jrico@ugto.mx, vperez@ugto.mx*

(Accepted January 28, 2015. First published online: February 24, 2015)

**SUMMARY**
This paper presents a systematic approach to compute the angularity and the axiality indices for a Schönflies parallel manipulator. *Angularity index* may be considered as a measure of the sensitivity of the mobile platform to changes in rotation, while *axiality index* can be used to measure the sensitivity of the OP of the mobile platform to changes in translation. Since both indices were inspired by very fundamental concepts of classical kinematics (angular velocity vector and helicoidal velocity field), they offer a clear and simple physical meaning, which may be useful to the designer of parallel manipulators. Moreover, both dexterity indices do not require obtaining a dimensionally homogeneous Jacobian matrix, nor do they depend on having similar types of actuators in each manipulator's leg. Detailed numerical examples are given in order to illustrate the computation of the dexterity indices.

KEYWORDS: Schönflies parallel manipulator; dexterity indices; angularity; axiality.

## 1. Introduction

Several dexterity indices have been proposed in order to design more efficient parallel manipulators, see Table 1 for a representative list. These indices are related to a number of concepts including the *condition number* of the Jacobian matrix,[1–4] *manipulability ellipsoid*,[5–7] examination of the Jacobian's *singular values*,[8] *rotation sensitivity,*[9] and *point-displacement sensitivity*.[9] In general, all these approaches are usually based on a first order (velocity) analysis whose typical form[4] is given by $\mathbf{F}\dot{\mathbf{x}} = \mathbf{G}\dot{\mathbf{q}}$, where $\dot{\mathbf{q}}$ is a vector containing the joint velocities of the actuated joints, $\mathbf{F}$ and $\mathbf{G}$ are the so-called *Jacobian matrices* of the manipulator, and $\dot{\mathbf{x}}$ is a vector associated with the velocity state of the mobile platform, that is, it may contain the angular velocity vector of the mobile platform and/or velocities of specially selected points pertaining to the mobile platform. In this context, it should be noted that, if the manipulator has a mix of revolute and prismatic actuators, or its mobile platform undergoes a general motion (translation and rotation), the Jacobian matrices $\mathbf{F}$ and $\mathbf{G}$ are usually *not homogeneous* in terms of units. Thus, the computation of the first five dexterity indices shown in Table 1 would mix translational and rotational capabilities, which is apparently meaningless.[2,7] Particularly important have been the efforts to *homogenize*[1,10–12] the Jacobian matrices. On the one hand, Gosselin[1] expressed the velocity vectors of three noncollinear points in a local coordinate frame which is rigidly attached to the mobile platform, but all the actuators were assumed to be of the revolute type. On the other hand, Kim and Ryu[10] proposed the use of the velocity vectors of three noncollinear points located on the planar mobile platform of a 6-DOF parallel manipulator, which is actuated by six prismatic actuators. In turn, the effort of Kong *et al.*[11] was focused on the use of the velocity vectors of three noncollinear points located on the planar mobile platform of a 6-DOF hybrid parallel manipulator, which is actuated by six revolute-type actuators. Finally, Liu *et al.*[12] resorted

* Corresponding author. E-mail: jecer@ugto.mx

Table I. Important features related to dexterity indices.

| | Requirement | |
|---|---|---|
| Dexterity index | Homogeneous Jacobian matrix | Similar actuator type |
| Condition number (Isotropy) | Yes | Yes |
| Rotation sensitivity | Yes | Yes |
| Point-displacement sensitivity | Yes | Yes |
| Manipulability ellipsoid | Yes | Yes |
| Jacobian's singular values | Yes | Yes |
| Angularity | No | No |
| Axiality | No | No |

to the use of five points and eight special axes associated with a virtual tetrahedron pertaining to the mobile platform of a parallel manipulator which is actuated with only one type of motor, either rotational or translational. However, although dimensionless Jacobian matrices are obtained, all the proposed approaches require that the parallel manipulator has only one type of actuator, which is a limitation to be taken into account.

In order to overcome the problem of dealing with nonhomogeneous Jacobian matrices, two novel dexterity indices have been recently introduced to estimate the motion performance of the mobile platform of a parallel manipulator undergoing a general motion.[13] On the one hand, the *angularity index* may be used to measure the sensitivity of the mobile platform to changes in rotation. On the other hand, the *axiality index* can be used to measure the sensitivity of the OP of the mobile platform to changes in translation. Since both indices were inspired by very fundamental concepts of classical kinematics (angular velocity vector and helicoidal velocity field), they offer a clear and simple physical meaning, which may be useful to the designer of parallel manipulators. Moreover, the proposed indices do not require obtaining a dimensionally homogeneous Jacobian matrix, nor do they depend on having similar types of actuators in each manipulator's leg. Hence, the objective of this paper is to apply the angularity and axiality indices to a particular Schönflies parallel manipulator in order to know about its kinematic performance.

## 2. The Schönflies Parallel Manipulator

In a recent work, Cervantes-Sánchez *et al.*[13] applied the angularity and axiality indices on a 3-PRS spatial parallel manipulator, which allows a combined motion of translation and rotation of its mobile platform. Now, the main objective of this paper is to apply the angularity and axiality indices to a different parallel manipulator. Therefore, it was selected a spatial parallel manipulator whose mobile platform has an interesting pattern motion, namely, a Schönflies motion, which is composed of three independent translations in space and one rotation about an axis with constant orientation. Thus, according to the approach proposed by Pérez-Soto *et al.*,[14] the manipulator under study was obtained by assembling four legs. These four legs include two types of basic legs proposed by Kong and Gosselin,[15] which were designed to generate a Schönflies motion. However, it is important to mention that this particular manipulator, as a whole, is not explicitly reported by Kong and Gosselin.[15]

On the other hand, one more reason to choose this manipulator was based on the fact that it is actuated by different types of actuators, namely, two rotational actuators and two translational actuators. In consequence, the application of the first five dexterity indices shown in Table 1 on the proposed Schönflies manipulator would face a major problem: the Jacobian matrices involved in their calculation are not homogeneous in terms of units. Therefore, only the angularity and axiality indices can be successfully applied to measure the kinematic dexterity of the Schönflies manipulator under study.

https://doi.org/10.1017/S0263574715000090 Published online by Cambridge University Press

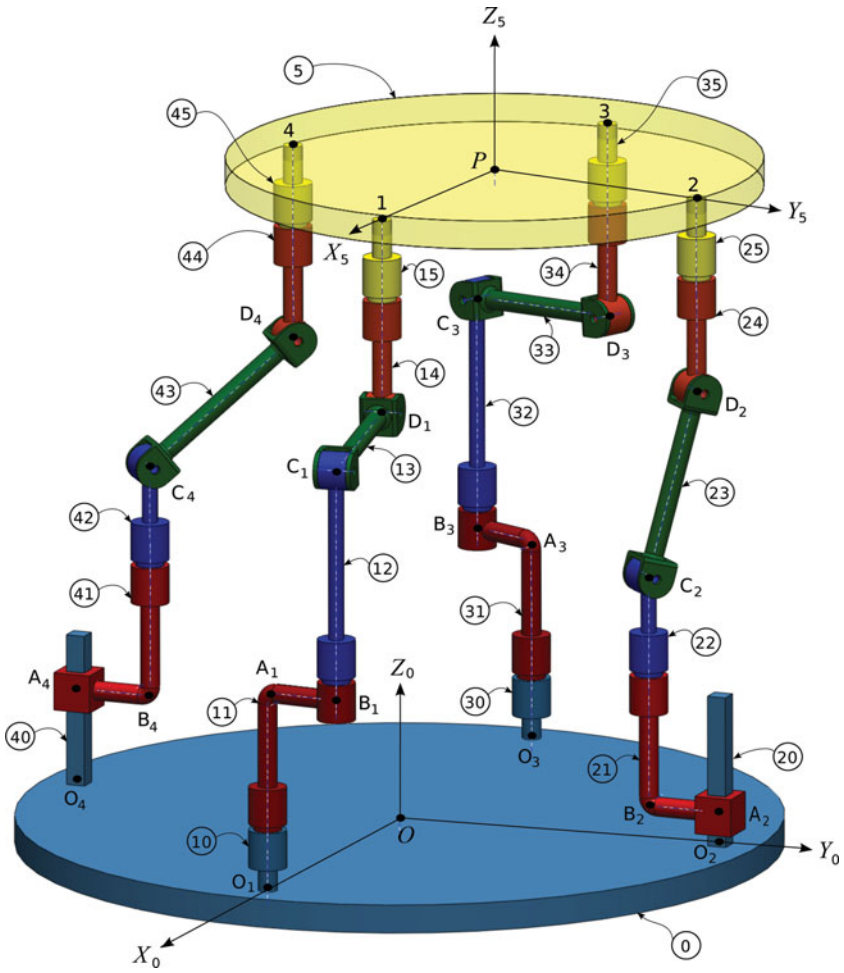


Fig. 1. Layout of the Schönflies parallel manipulator.

### *2.1. Kinematic architecture of the Schönflies parallel manipulator*

The Schönflies parallel manipulator under study is composed of four nonidentical five-degrees-of-freedom serial chains in a parallel array, sharing one common base (link 0) and one common moving platform (link 5), which is displayed in Fig. 1.

Referring to Fig. 1, *leg one* (links 10-11-12-13-14-15) and *leg three* (links 30-31-32-33-34-35) are made up of five revolute (R) joints. In this type of leg, the second and fifth joint axes are parallel to the first joint axis, whereas the fourth joint axis is parallel the third joint axis. Moreover, the third joint axis intersects the second perpendicularly, and the fifth joint axis intersects the fourth perpendicularly. Furthermore, a *rotational actuator* is used to drive the first joint of the leg where the motor is installed on the fixed platform.

On the other hand, *leg two* (links 20-21-22-23-24-25) and *leg four* (links 40-41-42-43-44-45) are built with one prismatic joint (P) and four revolute (R) joints. For this type of leg, the second and fifth joint axes are parallel to the first joint axis, whereas the fourth joint axis is parallel the third joint axis. Moreover, the third joint axis intersects the second perpendicularly, and the fifth joint axis intersects the fourth perpendicularly. Furthermore, the first moving link of this type of leg is driven by a *translational actuator* mounted on the fixed platform.

### *2.2. Geometry of the manipulator*

For the spatial parallel manipulator shown in Fig. 1, the four fixed points $O_1$, $O_2$, $O_3$, and $O_4$ define the geometry of the fixed platform, and the four moving points 1, 2, 3, and 4 define the geometry of the mobile platform.

https://doi.org/10.1017/S0263574715000090 Published online by Cambridge University Press

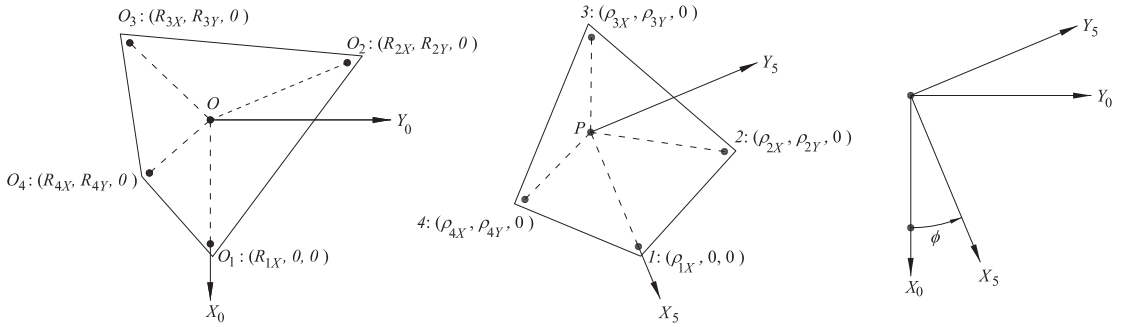


Fig. 2. General geometry of the fixed and mobile platforms.

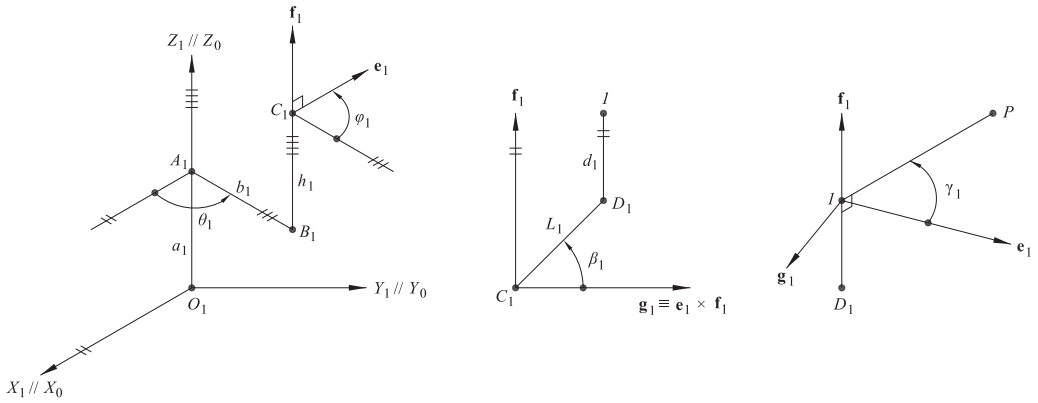


Fig. 3. Geometry of the first leg.

It should be noted that, although the particular manipulator's platforms shown in Fig. 1 are symmetrical, both platforms, the fixed platform and the mobile platform, may be *arbitrary quadrilaterals*, see Fig. 2.

On the other hand, Figs. 3–6 have been specially drawn in order show the link lengths and joint variables associated with the four manipulator's legs.

It is important to mention that unit vectors $\mathbf{e}_1$, $\mathbf{e}_2$, $\mathbf{e}_3$, and $\mathbf{e}_4$ denote the joint axes of those revolute joints that join links 12 and 13, 22 and 23, 32 and 33, and 42 and 43, respectively. Moreover, the pose of the mobile platform can be specified in terms of the position of point $P$, and an orientation angle, $\phi$. Furthermore, the origin of the fixed coordinate frame $X_0Y_0Z_0$ is located at point $O$.

## 3. Kinematic Position Analysis

In order to conduct a systematic numerical computation, a velocity analysis requires a previous kinematic position analysis. Basically, a *direct kinematic position analysis* (DKPA), is formulated in this section to achieve the objectives pursued in this paper. Firstly, it should be noted that angles $\varphi_1$, $\varphi_2$, $\varphi_3$, $\varphi_4$, $\beta_1$, $\beta_2$, $\beta_3$, $\beta_4$, $\gamma_1$, $\gamma_2$, $\gamma_3$, and $\gamma_4$ are *passive joint variables*, whereas $\theta_1$, $p_2$, $\theta_3$, and $p_4$ are *active joint variables*, see Figs. 3–6. On the other hand, vector $\mathbf{r}_{P/O} = (x, y, z)^T$ denotes the position vector of moving point $P$ with respect to fixed point $O$, which is measured in the $X_0Y_0Z_0$ coordinate frame, and $\phi$ denotes the rotation of the mobile platform about the $Z_0$ axis, see Fig. 2. Thus, the objective of the DKPA is to find the pose of the mobile platform, represented by $x$, $y$, $z$, and $\phi$, in terms of the actuator displacements $\theta_1$, $p_2$, $\theta_3$, and $p_4$.

### *3.1. Formulation of the constraint equations*

The formulation of the constraint equations begins by writing a loop-closure equation for each leg:

$$\mathbf{r}_{O_i/O} + \mathbf{r}_{A_i/O_i} + \mathbf{r}_{B_i/A_i} + \mathbf{r}_{C_i/B_i} + \mathbf{r}_{D_i/C_i} + \mathbf{r}_{i/D_i} = \mathbf{r}_{P/O} + \mathbf{r}_{i/P}, i = 1, 2, 3, 4, \tag{1}$$

where $\mathbf{r}_{j/k}$ stands for the position vector of point $j$ with respect to point $k$.

https://doi.org/10.1017/S0263574715000090 Published online by Cambridge University Press

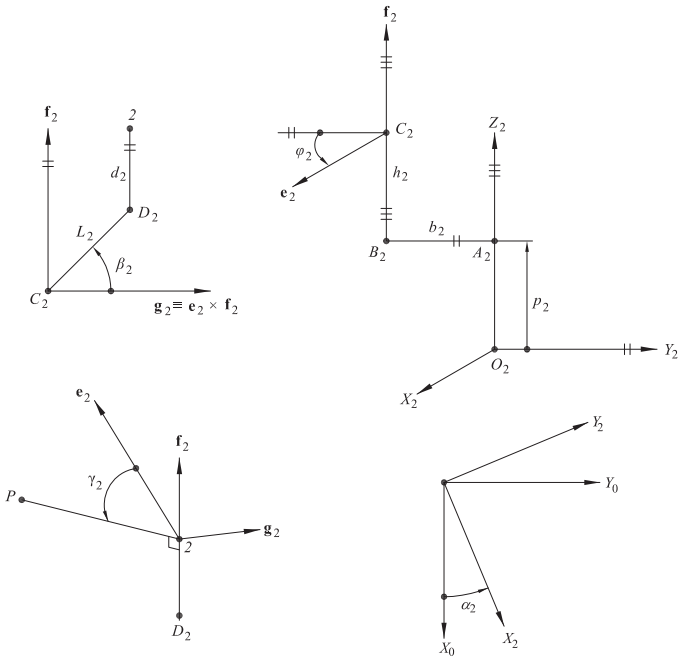


Fig. 4. Geometry of the second leg.

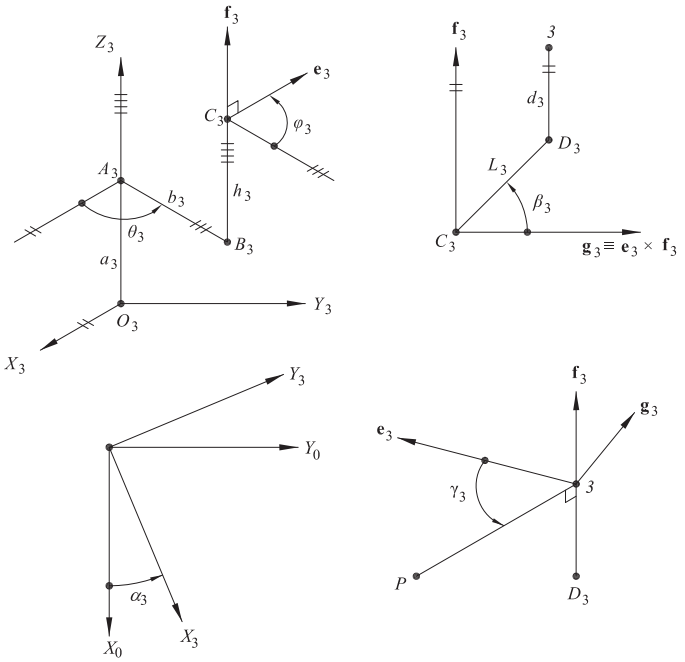


Fig. 5. Geometry of the third leg.

https://doi.org/10.1017/S0263574715000090 Published online by Cambridge University Press

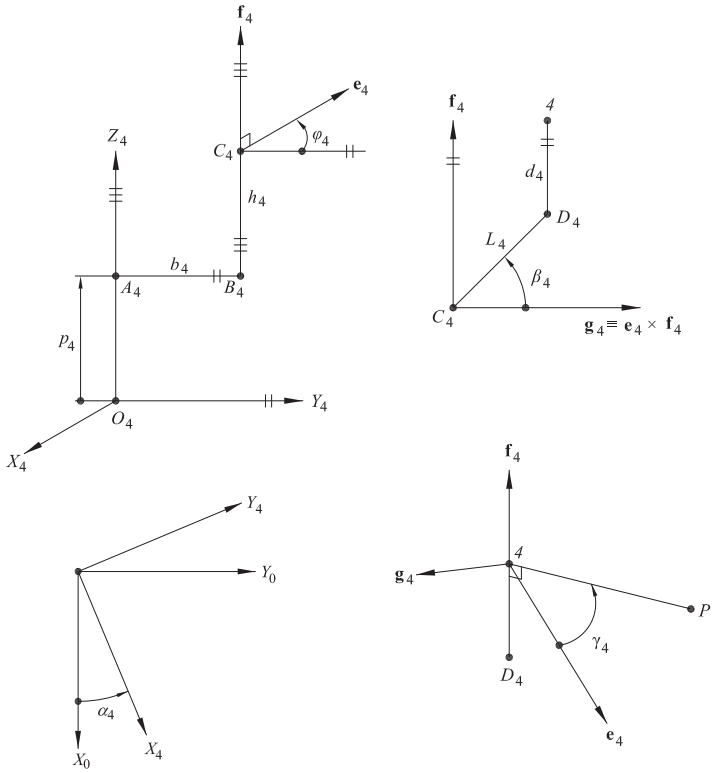


Fig. 6. Geometry of the fourth leg.

Writing Eq. (1) for $i = 1, 2, 3, 4$, and taking the $X_0Y_0Z_0$ coordinate frame as a reference, it is obtained that:

$$R_{1X} + b_1 \cos\theta_1 + L_1 \sin(\theta_1 + \varphi_1)\cos\beta_1 = x + \rho_{1X}\cos\phi \tag{2}$$

$$b_1 \sin\theta_1 - L_1 \cos(\theta_1 + \varphi_1)\cos\beta_1 = y + \rho_{1X}\sin\phi \tag{3}$$

$$a_1 + h_1 + L_1 \sin\beta_1 + d_1 = z \tag{4}$$

$$R_{2X} - L_2\cos\varphi_2\cos\beta_2\cos\alpha_2 + (b_2 + L_2\sin\varphi_2\cos\beta_2)\sin\alpha_2 = x + \rho_{2X}\cos\phi - \rho_{2Y}\sin\phi \tag{5}$$

$$R_{2Y} - L_2\cos\varphi_2\cos\beta_2\sin\alpha_2 - (b_2 + L_2\sin\varphi_2\cos\beta_2)\cos\alpha_2 = y + \rho_{2X}\sin\phi + \rho_{2Y}\cos\phi \tag{6}$$

$$p_2 + h_2 + L_2\sin\beta_2 + d_2 = z \tag{7}$$

$$\begin{aligned} &R_{3X} + \{b_3\cos\theta_3 + L_3\sin(\theta_3 + \varphi_3)\cos\beta_3\}\cos\alpha_3 \\ &\quad - \{b_3\sin\theta_3 - L_3\cos(\theta_3 + \varphi_3)\cos\beta_3\}\sin\alpha_3 = x + \rho_{3X}\cos\phi - \rho_{3Y}\sin\phi \end{aligned} \tag{8}$$

$$\begin{aligned} &R_{3Y} + \{b_3\cos\theta_3 + L_3\sin(\theta_3 + \varphi_3)\cos\beta_3\}\sin\alpha_3 \\ &\quad + \{b_3\sin\theta_3 - L_3\cos(\theta_3 + \varphi_3)\cos\beta_3\}\cos\alpha_3 = y + \rho_{3X}\sin\phi + \rho_{3Y}\cos\phi \end{aligned} \tag{9}$$

$$a_3 + h_3 + L_3\sin\beta_3 + d_3 = z \tag{10}$$

$$R_{4X} + L_4\cos\varphi_4\cos\beta_4\cos\alpha_4 - (b_4 + L_4\sin\varphi_4\cos\beta_4)\sin\alpha_4 = x + \rho_{4X}\cos\phi - \rho_{4Y}\sin\phi \tag{11}$$

$$R_{4Y} + L_4\cos\varphi_4\cos\beta_4\sin\alpha_4 + (b_4 + L_4\sin\varphi_4\cos\beta_4)\cos\alpha_4 = y + \rho_{4X}\sin\phi + \rho_{4Y}\cos\phi \tag{12}$$

$$p_4 + h_4 + L_4\sin\beta_4 + d_4 = z \tag{13}$$

which are the *constraint equations* sought.

https://doi.org/10.1017/S0263574715000090 Published online by Cambridge University Press

*3.2. Solution of the direct kinematic position problem*

The solution of the kinematic position problem can be started by realizing that Eqs. (2)–(13) are linear in the sines and cosines of passive joint variables $\varphi_1$, $\varphi_2$, $\varphi_3$, and $\varphi_4$. Thus, from simultaneous solution of Eqs. (2), and (3), (5), and (6), (8), and (9), (11), and (12), respectively, it is found that:

$$\sin\varphi_1 = \frac{\rho_{1X}\cos(\phi-\theta_1)+(x-R_{1X})\cos\theta_1+y\sin\theta_1-b_1}{L_1\cos\beta_1} \tag{14}$$

$$\cos\varphi_1 = \frac{-\rho_{1X}\sin(\phi-\theta_1)+(x-R_{1X})\sin\theta_1-y\cos\theta_1}{L_1\cos\beta_1} \tag{15}$$

$$\sin\varphi_2 = \frac{-\rho_{2X}\sin(\phi-\alpha_2)-\rho_{2Y}\cos(\phi-\alpha_2)-R_{2X}\sin\alpha_2+R_{2Y}\cos\alpha_2+x\sin\alpha_2-y\cos\alpha_2-b_2}{L_2\cos\beta_2} \tag{16}$$

$$\cos\varphi_2 = \frac{-\rho_{2X}\cos(\phi-\alpha_2)+\rho_{2Y}\sin(\phi-\alpha_2)+R_{2X}\cos\alpha_2+R_{2Y}\sin\alpha_2-x\cos\alpha_2-y\sin\alpha_2}{L_2\cos\beta_2} \tag{17}$$

$$\sin\varphi_3 = \frac{\rho_{3X}\cos(\phi-\theta_3-\alpha_3)-\rho_{3Y}\sin(\phi-\theta_3-\alpha_3)}{L_3\cos\beta_3} - \frac{R_{3X}\cos(\theta_3+\alpha_3)+R_{3Y}\sin(\theta_3+\alpha_3)-x\cos(\theta_3+\alpha_3)-y\sin(\theta_3+\alpha_3)+b_3}{L_3\cos\beta_3} \tag{18}$$

$$\cos\varphi_3 = -\frac{\rho_{3X}\sin(\phi-\theta_3-\alpha_3)+\rho_{3Y}\cos(\phi-\theta_3-\alpha_3)}{L_3\cos\beta_3} + \frac{-R_{3X}\sin(\theta_3+\alpha_3)+R_{3Y}\cos(\theta_3+\alpha_3)+x\sin(\theta_3+\alpha_3)-y\cos(\theta_3+\alpha_3)}{L_3\cos\beta_3} \tag{19}$$

$$\sin\varphi_4 = \frac{\rho_{4X}\sin(\phi-\alpha_4)+\rho_{4Y}\cos(\phi-\alpha_4)+R_{4X}\sin\alpha_4-R_{4Y}\cos\alpha_4-x\sin\alpha_4+y\cos\alpha_4-b_4}{L_4\cos\beta_4} \tag{20}$$

$$\cos\varphi_4 = \frac{\rho_{4X}\cos(\phi-\alpha_4)-\rho_{4Y}\sin(\phi-\alpha_4)-R_{4X}\cos\alpha_4-R_{4Y}\sin\alpha_4+x\cos\alpha_4+y\sin\alpha_4}{L_4\cos\beta_4}. \tag{21}$$

Introducing the trigonometric identities $\sin^2\varphi_i+\cos^2\varphi_i=1$, for $i = 1, 2, 3,$ and 4, Eqs. (14)–(21) become:

$$\begin{aligned}
&2\rho_{1X}\{x\cos\phi+y\sin\phi-b_1\cos(\phi-\theta_1)-R_{1X}\cos\phi+\rho_{1X}/2\}\\
&\quad-2b_1(x\cos\theta_1+y\sin\theta_1-R_{1X}\cos\theta_1)\\
&\quad+(R_{1X}-x)^2+y^2+b_1^2-L_1^2\cos^2\beta_1=0
\end{aligned} \tag{22}$$

$$\begin{aligned}
&2\rho_{2X}\{x\cos\phi+y\sin\phi+b_2\sin(\phi-\alpha_2)-R_{2X}\cos\phi-R_{2Y}\sin\phi+\rho_{2X}/2\}\\
&\quad-2\rho_{2Y}\{x\sin\phi-y\cos\phi-b_2\cos(\phi-\alpha_2)-R_{2X}\sin\phi+R_{2Y}\cos\phi-\rho_{2Y}/2\}\\
&\quad-2b_2\{x\sin\alpha_2-y\cos\alpha_2-R_{2X}\sin\alpha_2+R_{2Y}\cos\alpha_2-b_2/2\}\\
&\quad+(R_{2X}-x)^2+(R_{2Y}-y)^2-L_2^2\cos^2\beta_2=0
\end{aligned} \tag{23}$$

https://doi.org/10.1017/S0263574715000090 Published online by Cambridge University Press

$$
\begin{aligned}
&2\rho_{3X}\{x\cos\phi + y\sin\phi - b_3\cos(\phi-\theta_3-\alpha_3) - R_{3X}\cos\phi - R_{3Y}\sin\phi + \rho_{3X}/2\}\\
&\quad - 2\rho_{3Y}\{x\sin\phi - y\cos\phi - b_3\sin(\phi-\theta_3-\alpha_3) - R_{3X}\sin\phi + R_{3Y}\cos\phi - \rho_{3Y}/2\}\\
&\quad - 2b_3\{x\cos(\theta_3+\alpha_3) + y\sin(\theta_3+\alpha_3) - R_{3X}\cos(\theta_3+\alpha_3) - R_{3Y}\sin(\theta_3+\alpha_3) - b_3/2\}\\
&\quad + (R_{3X}-x)^2 + (R_{3Y}-y)^2 - L_3^2\cos^2\beta_3 = 0 \qquad (24)\\
&2\rho_{4X}\{x\cos\phi + y\sin\phi - b_4\sin(\phi-\alpha_4) - R_{4X}\cos\phi - R_{4Y}\sin\phi + \rho_{4X}/2\}\\
&\quad - 2\rho_{4Y}\{x\sin\phi - y\cos\phi + b_4\cos(\phi-\alpha_4) - R_{4X}\sin\phi + R_{4Y}\cos\phi - \rho_{4Y}/2\}\\
&\quad + 2b_4\{x\sin\alpha_4 - y\cos\alpha_4 - R_{4X}\sin\alpha_4 + R_{4Y}\cos\alpha_4 + b_4/2\}\\
&\quad + (R_{4X}-x)^2 + (R_{4Y}-y)^2 - L_4^2\cos^2\beta_4 = 0. \qquad (25)
\end{aligned}
$$

Now, Eqs. (4), (7), (10), and (13) are solved for $\sin\beta_1$, $\sin\beta_2$, $\sin\beta_3$, and $\sin\beta_4$, respectively, and then squared. Next, Eqs. (22)–(25) are solved for $\cos^2\beta_1$, $\cos^2\beta_2$, $\cos^2\beta_3$, and $\cos^2\beta_4$, respectively. Thus, by introducing the trigonometric identities $\sin^2\beta_i + \cos^2\beta_i = 1$, for $i = 1, 2, 3, 4$, the following equations are obtained:

$$x^2 + y^2 + z^2 + k_{11}x + k_{12}y + k_{13}z + k_{14} = 0 \qquad (26)$$

$$x^2 + y^2 + z^2 + k_{21}x + k_{22}y + k_{23}z + k_{24} = 0 \qquad (27)$$

$$x^2 + y^2 + z^2 + k_{31}x + k_{32}y + k_{33}z + k_{34} = 0 \qquad (28)$$

$$x^2 + y^2 + z^2 + k_{41}x + k_{42}y + k_{43}z + k_{44} = 0 \qquad (29)$$

which is a system composed of four nonlinear Eqs. (26)–(29) in four unknowns, $x$, $y$, $z$, and $\phi$. In fact, angle $\phi$ appears in parameters $k_{ij}$, which are given by:

$$
\begin{aligned}
k_{11} &\equiv 2\rho_{1X}\cos\phi - 2b_1\cos\theta_1 - 2R_{1X}\\
k_{12} &\equiv 2\rho_{1X}\sin\phi - 2b_1\sin\theta_1\\
k_{13} &\equiv -2(a_1 + d_1 + h_1)\\
k_{14} &\equiv 2b_1\{R_{1X}\cos\theta_1 - \rho_{1X}\cos(\phi-\theta_1)\} - 2R_{1X}\rho_{1X}\cos\phi + (a_1+d_1+h_1)^2 + b_1^2\\
&\quad + R_{1X}^2 + \rho_{1X}^2 - L_1^2\\
k_{21} &\equiv 2\rho_{2X}\cos\phi - 2\rho_{2Y}\sin\phi - 2b_2\sin\alpha_2 - 2R_{2X}\\
k_{22} &\equiv 2\rho_{2X}\sin\phi + 2\rho_{2Y}\cos\phi + 2b_2\cos\alpha_2 - 2R_{2Y}\\
k_{23} &\equiv -2(p_2 + d_2 + h_2)\\
k_{24} &\equiv 2b_2\{\rho_{2X}\sin(\phi-\alpha_2) + \rho_{2Y}\cos(\phi-\alpha_2)\\
&\quad + R_{2X}\sin\alpha_2 - R_{2Y}\cos\alpha_2\}\\
&\quad + 2R_{2X}\{\rho_{2Y}\sin\phi - \rho_{2X}\cos\phi\} - 2R_{2Y}\{\rho_{2X}\sin\phi + \rho_{2Y}\cos\phi\}\\
&\quad + (p_2+d_2+h_2)^2 + b_2^2 + R_{2X}^2 + R_{2Y}^2 + \rho_{2X}^2 + \rho_{2Y}^2 - L_2^2.\\
k_{31} &\equiv 2\rho_{3X}\cos\phi - 2\rho_{3Y}\sin\phi - 2b_3\cos(\theta_3+\alpha_3) - 2R_{3X}\\
k_{32} &\equiv 2\rho_{3X}\sin\phi + 2\rho_{3Y}\cos\phi - 2b_3\sin(\theta_3+\alpha_3) - 2R_{3Y}\\
k_{33} &\equiv -2(a_3 + d_3 + h_3)\\
k_{34} &\equiv 2b_3\{-\rho_{3X}\cos(\phi-\theta_3-\alpha_3) + \rho_{3Y}\sin(\phi-\theta_3-\alpha_3) + R_{3X}\cos(\theta_3+\alpha_3) + R_{3Y}\sin(\theta_3+\alpha_3)\}\\
&\quad + 2R_{3X}\{\rho_{3Y}\sin\phi - \rho_{3X}\cos\phi\} - 2R_{3Y}\{\rho_{3X}\sin\phi + \rho_{3Y}\cos\phi\}\\
&\quad + (a_3+d_3+h_3)^2 + b_3^2 + R_{3X}^2 + R_{3Y}^2 + \rho_{3X}^2 + \rho_{3Y}^2 - L_3^2.
\end{aligned}
$$

https://doi.org/10.1017/S0263574715000090 Published online by Cambridge University Press

$$
\begin{aligned}
k_{41} &\equiv 2\rho_{4X}\cos\phi - 2\rho_{4Y}\sin\phi + 2b_4\sin\alpha_4 - 2R_{4X}\\
k_{42} &\equiv 2\rho_{4X}\sin\phi + 2\rho_{4Y}\cos\phi - 2b_4\cos\alpha_4 - 2R_{4Y}\\
k_{43} &\equiv -2(p_4 + d_4 + h_4)\\
k_{44} &\equiv 2b_4\{-\rho_{4X}\sin(\phi-\alpha_4) - \rho_{4Y}\cos(\phi-\alpha_4) - R_{4X}\sin\alpha_4 + R_{4Y}\cos\alpha_4\}\\
&\quad + 2R_{4X}\{\rho_{4Y}\sin\phi - \rho_{4X}\cos\phi\} - 2R_{4Y}\{\rho_{4X}\sin\phi + \rho_{4Y}\cos\phi\}\\
&\quad + (p_4 + d_4 + h_4)^2 + b_4^2 + R_{4X}^2 + R_{4Y}^2 + \rho_{4X}^2 + \rho_{4Y}^2 - L_4^2.
\end{aligned}
$$

System of Eqs. (26)–(29) can be simplified by performing the following operations. Subtracting Eqs. (27)–(29) from Eq. (26) yields:

$$(k_{11}-k_{21})x + (k_{12}-k_{22})y + (k_{13}-k_{23})z + k_{14} - k_{24} = 0 \tag{30}$$

$$(k_{11}-k_{31})x + (k_{12}-k_{32})y + (k_{13}-k_{33})z + k_{14} - k_{34} = 0 \tag{31}$$

$$(k_{11}-k_{41})x + (k_{12}-k_{42})y + (k_{13}-k_{43})z + k_{14} - k_{44} = 0. \tag{32}$$

Equations (30)–(32) can be written in the following matrix form:

$$\left[\mathbf{u}_1\ \mathbf{u}_2\ \mathbf{u}_3\right]\mathbf{p} = \mathbf{b}, \quad \mathbf{U}\mathbf{p} = \mathbf{b}, \tag{33}$$

where:

$$
\mathbf{u}_1 \equiv \begin{bmatrix} k_{11}-k_{21} \\ k_{11}-k_{31} \\ k_{11}-k_{41} \end{bmatrix}, \quad
\mathbf{u}_2 \equiv \begin{bmatrix} k_{12}-k_{22} \\ k_{12}-k_{32} \\ k_{12}-k_{42} \end{bmatrix}, \quad
\mathbf{u}_3 \equiv \begin{bmatrix} k_{13}-k_{23} \\ k_{13}-k_{33} \\ k_{13}-k_{43} \end{bmatrix},
$$

$$
\mathbf{p} \equiv \mathbf{r}_{P/O} = \begin{bmatrix} x \\ y \\ z \end{bmatrix}, \quad
\mathbf{b} \equiv \begin{bmatrix} k_{24}-k_{14} \\ k_{34}-k_{14} \\ k_{44}-k_{14} \end{bmatrix}.
$$

Equation (33) may be symbolically solved as follows:

$$\mathbf{p} = \mathbf{U}^{-1}\mathbf{b}, \tag{34}$$

where inverse matrix $\mathbf{U}^{-1}$ may be expressed in terms of its columns explicitly, without introducing components:[16,17]

$$\mathbf{U}^{-1} = \frac{1}{(\mathbf{u}_1 \times \mathbf{u}_2)\cdot\mathbf{u}_3}\begin{bmatrix} (\mathbf{u}_2 \times \mathbf{u}_3)^T \\ (\mathbf{u}_3 \times \mathbf{u}_1)^T \\ (\mathbf{u}_1 \times \mathbf{u}_2)^T \end{bmatrix}. \tag{35}$$

Equations (34) and (35) are now combined to yield:

$$x = \frac{(\mathbf{u}_2 \times \mathbf{u}_3)\cdot\mathbf{b}}{(\mathbf{u}_1 \times \mathbf{u}_2)\cdot\mathbf{u}_3} \tag{36}$$

$$y = \frac{(\mathbf{u}_3 \times \mathbf{u}_1)\cdot\mathbf{b}}{(\mathbf{u}_1 \times \mathbf{u}_2)\cdot\mathbf{u}_3} \tag{37}$$

$$z = \frac{(\mathbf{u}_1 \times \mathbf{u}_2)\cdot\mathbf{b}}{(\mathbf{u}_1 \times \mathbf{u}_2)\cdot\mathbf{u}_3}. \tag{38}$$

https://doi.org/10.1017/S0263574715000090 Published online by Cambridge University Press

If Eqs. (36)–(38) are substituted into any of Eqs. (26)–(29), a 12th-degree polynomial in $\tau$ is obtained:

$$m_{12}\tau^{12} + m_{11}\tau^{11} + m_{10}\tau^{10} + m_9\tau^9 + m_8\tau^8 + m_7\tau^7 + m_6\tau^6 + m_5\tau^5 + m_4\tau^4 + m_3\tau^3 + m_2\tau^2 + m_1\tau + m_0 = 0, \tag{39}$$

where $\tau \equiv \tan(\frac{\phi}{2})$. Because of all the coefficients $m_0, m_1, \ldots, m_{12}$ depend only on the input displacements, namely, $\theta_1$, $p_2$, $\theta_3$, and $p_4$, Eq. (39) may be considered as a *closed form solution* for $\phi$.

### *3.3. Vector solution of the loop-closure equations*

The loop-closure Eq. (1) can be solved as follows:

$$\mathbf{r}_{D_i/C_i} = \mathbf{r}_{P/O} + \mathbf{r}_{i/P} - \mathbf{r}_{O_i/O} - \mathbf{r}_{A_i/O_i} - \mathbf{r}_{B_i/A_i} - \mathbf{r}_{C_i/B_i} - \mathbf{r}_{i/D_i}, \; i = 1, 2, 3, 4. \tag{40}$$

Thus, based on the geometry shown in Figs. 3–6, and, if the fixed coordinate system $X_0Y_0Z_0$ is taken as reference, Eq. (40) leads to:

$$\mathbf{r}_{D_1/C_1} = \begin{bmatrix} x + \rho_{1X}\cos\phi - b_1\cos\theta_1 - R_{1X} \\ y + \rho_{1X}\sin\phi - b_1\sin\theta_1 \\ z - a_1 - h_1 - d_1 \end{bmatrix} \tag{41}$$

$$\mathbf{r}_{D_2/C_2} = \begin{bmatrix} x + \rho_{2X}\cos\phi - \rho_{2Y}\sin\phi - R_{2X} - b_2\sin\alpha_2 \\ y + \rho_{2X}\sin\phi + \rho_{2Y}\cos\phi - R_{2Y} + b_2\cos\alpha_2 \\ z - p_2 - h_2 - d_2 \end{bmatrix} \tag{42}$$

$$\mathbf{r}_{D_3/C_3} = \begin{bmatrix} x + \rho_{3X}\cos\phi - \rho_{3Y}\sin\phi - b_3\cos\alpha_3\cos\theta_3 + b_3\sin\alpha_3\sin\theta_3 - R_{3X} \\ y + \rho_{3X}\sin\phi + \rho_{3Y}\cos\phi - b_3\sin\alpha_3\cos\theta_3 - b_3\cos\alpha_3\sin\theta_3 - R_{3Y} \\ z - a_3 - h_3 - d_3 \end{bmatrix} \tag{43}$$

$$\mathbf{r}_{D_4/C_4} = \begin{bmatrix} x + \rho_{4X}\cos\phi - \rho_{4Y}\sin\phi + b_4\sin\alpha_4 - R_{4X} \\ y + \rho_{4X}\sin\phi + \rho_{4Y}\cos\phi - b_4\cos\alpha_4 - R_{4Y} \\ z - p_4 - h_4 - d_4 \end{bmatrix}. \tag{44}$$

At this point it is important to realize that input displacements $\theta_1$, $p_2$, $\theta_3$, and $p_4$, are implicitly related to position vectors $\mathbf{r}_{D_1/C_1}$, $\mathbf{r}_{D_2/C_2}$, $\mathbf{r}_{D_3/C_3}$, and $\mathbf{r}_{D_4/C_4}$, through Eqs. (41)–(44), respectively. Moreover, values of angle $\phi$ and Cartesian coordinates $x$, $y$, and $z$, can be computed from Eqs. (39), (36), (37), and (38), respectively. The relevance of computing position vectors $\mathbf{r}_{D_1/C_1}$, $\mathbf{r}_{D_2/C_2}$, $\mathbf{r}_{D_3/C_3}$, and $\mathbf{r}_{D_4/C_4}$ will be evident in the following sections.

## 4. Velocity Analysis

The goal of this section is to solve the *direct kinematic velocity problem*. Therefore, given the *input joint velocities* of the Schönflies manipulator, namely, $\dot{\mathbf{q}}_I \equiv (\dot{\theta}_1, \dot{p}_2, \dot{\theta}_3, \dot{p}_4)^T$, it is required to compute the velocity state of the mobile platform, namely, $\mathbf{V}_{5/0} \equiv (\boldsymbol{\omega}_{5/0}, \mathbf{v}_{P/O})^T$, where $\mathbf{v}_{P/O} = (\dot{x}, \dot{y}, \dot{z})^T$ is the velocity vector of point $P$, $\boldsymbol{\omega}_{5/0} = \dot{\phi}\,\mathbf{k}_0$ is the angular velocity vector of the mobile platform, and $\mathbf{k}_0$ is a unit vector along axis $Z_0$.

https://doi.org/10.1017/S0263574715000090 Published online by Cambridge University Press

Firstly, by means of a velocity analysis, it can be obtained the following relationship between the input and the output velocities:

$$\begin{bmatrix} \mu_1 & \mathbf{r}_{D_1/C_1}^T \\ \mu_2 & \mathbf{r}_{D_2/C_2}^T \\ \mu_3 & \mathbf{r}_{D_3/C_3}^T \\ \mu_4 & \mathbf{r}_{D_4/C_4}^T \end{bmatrix} \begin{bmatrix} \dot{\phi} \\ \mathbf{v}_{P/O} \end{bmatrix} = \begin{bmatrix} \lambda_1 & 0 & 0 & 0 \\ 0 & \lambda_2 & 0 & 0 \\ 0 & 0 & \lambda_3 & 0 \\ 0 & 0 & 0 & \lambda_4 \end{bmatrix} \begin{bmatrix} \dot{\theta}_1 \\ \dot{p}_2 \\ \dot{\theta}_3 \\ \dot{p}_4 \end{bmatrix}, \quad \mathbf{A}\dot{\mathbf{s}} = \mathbf{B}\dot{\mathbf{q}}_I \tag{45}$$

where:

$$\begin{aligned} \mu_1 &\equiv (\mathbf{k}_0 \times \mathbf{r}_{1/P}) \cdot \mathbf{r}_{D_1/C_1}, & \lambda_1 &\equiv (\mathbf{k}_0 \times \mathbf{r}_{B_1/A_1}) \cdot \mathbf{r}_{D_1/C_1}, \\ \mu_2 &\equiv (\mathbf{k}_0 \times \mathbf{r}_{2/P}) \cdot \mathbf{r}_{D_2/C_2}, & \lambda_2 &\equiv \mathbf{k}_0 \cdot \mathbf{r}_{D_2/C_2}, \\ \mu_3 &\equiv (\mathbf{k}_0 \times \mathbf{r}_{3/P}) \cdot \mathbf{r}_{D_3/C_3}, & \lambda_3 &\equiv (\mathbf{k}_0 \times \mathbf{r}_{B_3/A_3}) \cdot \mathbf{r}_{D_3/C_3}, \\ \mu_4 &\equiv (\mathbf{k}_0 \times \mathbf{r}_{4/P}) \cdot \mathbf{r}_{D_4/C_4}, & \lambda_4 &\equiv \mathbf{k}_0 \cdot \mathbf{r}_{D_4/C_4}, \end{aligned}$$

with:

$$\mathbf{r}_{1/P} = \begin{bmatrix} \rho_{1X} \cos\phi \\ \rho_{1X} \sin\phi \\ 0 \end{bmatrix}, \quad \mathbf{r}_{2/P} = \begin{bmatrix} \rho_{2X} \cos\phi - \rho_{2Y} \sin\phi \\ \rho_{2X} \sin\phi + \rho_{2Y} \cos\phi \\ 0 \end{bmatrix} \tag{46}$$

$$\mathbf{r}_{3/P} = \begin{bmatrix} \rho_{3X} \cos\phi - \rho_{3Y} \sin\phi \\ \rho_{3X} \sin\phi + \rho_{3Y} \cos\phi \\ 0 \end{bmatrix}, \quad \mathbf{r}_{4/P} = \begin{bmatrix} \rho_{4X} \cos\phi - \rho_{4Y} \sin\phi \\ \rho_{4X} \sin\phi + \rho_{4Y} \cos\phi \\ 0 \end{bmatrix} \tag{47}$$

$$\mathbf{r}_{B_1/A_1} = \begin{bmatrix} b_1 \cos\theta_1 \\ b_1 \sin\theta_1 \\ 0 \end{bmatrix}, \quad \mathbf{r}_{B_3/A_3} = \begin{bmatrix} b_3 \cos\alpha_3 \cos\theta_3 - b_3 \sin\alpha_3 \sin\theta_3 \\ b_3 \sin\alpha_3 \cos\theta_3 + b_3 \cos\alpha_3 \sin\theta_3 \\ 0 \end{bmatrix}. \tag{48}$$

It should be noted that all the position vectors involved in the coefficients $\mu_1$, $\mu_2$, $\mu_3$, $\mu_4$, $\lambda_1$, $\lambda_2$, $\lambda_3$, and $\lambda_4$, can be readily computed by resorting to Eqs. (41)–(44), and (46)–(48).

### *4.1. Velocity vector of point* P

The objective of this section is to obtain an explicit equation for the velocity vector of point $P$ in terms of the input joint velocities $\dot{\mathbf{q}}_I \equiv (\dot{\theta}_1, \dot{p}_2, \dot{\theta}_3, \dot{p}_4)^T$. To this end, Eq. (45) can be rearranged as follows:

$$\mathbf{v}_{P/O} \cdot \mathbf{r}_{D_1/C_1} + \mu_1 \dot{\phi} = \lambda_1 \dot{\theta}_1 \tag{49}$$

$$\mathbf{v}_{P/O} \cdot \mathbf{r}_{D_2/C_2} + \mu_2 \dot{\phi} = \lambda_2 \dot{p}_2 \tag{50}$$

$$\mathbf{v}_{P/O} \cdot \mathbf{r}_{D_3/C_3} + \mu_3 \dot{\phi} = \lambda_3 \dot{\theta}_3 \tag{51}$$

$$\mathbf{v}_{P/O} \cdot \mathbf{r}_{D_4/C_4} + \mu_4 \dot{\phi} = \lambda_4 \dot{p}_4. \tag{52}$$

Successive elimination of $\dot{\phi}$ from Eqs. (49)–(52) leads to:

$$\begin{bmatrix} \mathbf{m}_1^T \\ \mathbf{m}_2^T \\ \mathbf{m}_3^T \end{bmatrix} \mathbf{v}_{P/O} = \begin{bmatrix} \mu_2\lambda_1 & -\mu_1\lambda_2 & 0 & 0 \\ \mu_3\lambda_1 & 0 & -\mu_1\lambda_3 & 0 \\ \mu_4\lambda_1 & 0 & 0 & -\mu_1\lambda_4 \end{bmatrix} \begin{bmatrix} \dot{\theta}_1 \\ \dot{p}_2 \\ \dot{\theta}_3 \\ \dot{p}_4 \end{bmatrix}, \quad \mathbf{M}\mathbf{v}_{P/O} = \mathbf{N}\dot{\mathbf{q}}_I, \tag{53}$$

https://doi.org/10.1017/S0263574715000090 Published online by Cambridge University Press

where:

$$\mathbf{m}_1 \equiv \mu_2 \mathbf{r}_{D_1/C_1} - \mu_1 \mathbf{r}_{D_2/C_2}$$
$$\mathbf{m}_2 \equiv \mu_3 \mathbf{r}_{D_1/C_1} - \mu_1 \mathbf{r}_{D_3/C_3}$$
$$\mathbf{m}_3 \equiv \mu_4 \mathbf{r}_{D_1/C_1} - \mu_1 \mathbf{r}_{D_4/C_4}.$$

Assuming that matrix $\mathbf{M}$ is nonsingular, then Eq. (53) can be transformed into:

$$\mathbf{v}_{P/O} = (\mathbf{M}^{-1}\mathbf{N})\dot{\mathbf{q}}_I, \tag{54}$$

where, inverse matrix is given by:[16,17]

$$\mathbf{M}^{-1} = \left(\frac{1}{\mathbf{m}_1 \cdot (\mathbf{m}_2 \times \mathbf{m}_3)}\right)[\,\mathbf{m}_2 \times \mathbf{m}_3 \quad \mathbf{m}_3 \times \mathbf{m}_1 \quad \mathbf{m}_1 \times \mathbf{m}_2\,]. \tag{55}$$

Thus, Eq. (54) provides the result sought.

*4.2. Angular velocity of the mobile platform*

Since the mobile platform rotates about $Z_0$ axis, its angular velocity vector is given by $\boldsymbol{\omega}_{5/0} = \dot{\phi}\,\mathbf{k}_0$. Thus, once $\mathbf{v}_{P/O}$ is known, the angular velocity scalar $\dot{\phi}$ can be computed from any of Eqs. (49)–(52), that is:

$$\dot{\phi} = \frac{\lambda_i \dot{\theta}_i - \mathbf{v}_{P/O} \cdot \mathbf{r}_{D_i/C_i}}{\mu_i} = \frac{\lambda_j \dot{p}_j - \mathbf{v}_{P/O} \cdot \mathbf{r}_{D_j/C_j}}{\mu_j}, \quad i = 1, 3, \text{ and } j = 2, 4, \tag{56}$$

thus having four options to choose.

*4.3. Velocity of the attachment points*

An *attachment point* is usually located at the physical center of the joint that connects the terminal link of a leg with the mobile platform. Thus, for the parallel manipulator under study, there are four attachment points, namely, points 1, 2, 3, and 4, see Figs. 1–2.

From basic concepts of rigid body kinematics, the following equations can be readily formulated:

$$\mathbf{v}_{1/O} \equiv \mathbf{v}_1 = \mathbf{v}_{P/O} + \boldsymbol{\omega}_{5/0} \times \mathbf{r}_{1/P} \tag{57}$$
$$\mathbf{v}_{2/O} \equiv \mathbf{v}_2 = \mathbf{v}_{P/O} + \boldsymbol{\omega}_{5/0} \times \mathbf{r}_{2/P} \tag{58}$$
$$\mathbf{v}_{3/O} \equiv \mathbf{v}_3 = \mathbf{v}_{P/O} + \boldsymbol{\omega}_{5/0} \times \mathbf{r}_{3/P} \tag{59}$$
$$\mathbf{v}_{4/O} \equiv \mathbf{v}_4 = \mathbf{v}_{P/O} + \boldsymbol{\omega}_{5/0} \times \mathbf{r}_{4/P}, \tag{60}$$

where position vectors $\mathbf{r}_{1/P}$, $\mathbf{r}_{2/P}$, $\mathbf{r}_{3/P}$, and $\mathbf{r}_{4/P}$ are given by Eqs. (46)–(47). Thus, a systematic computation of the velocity vectors of the attachment points can be readily performed by resorting to Eqs. (57)–(60).

## 5. Angularity Index

The *angularity index* can be used as a measure to estimate the manipulator's ability to convert the velocity of the legs—characterized by the velocities of the attachment points—into the angular velocity of the mobile platform.[13] This index is denoted by Greek symbol $\eta$, and it is defined as follows:

$$\eta = \frac{\|\mathbf{v}_{21} \times \mathbf{v}_{31}\|}{\|\mathbf{v}_{21}\|\|\mathbf{v}_{31}\|}, \quad 0 \le \eta \le 1, \tag{61}$$

https://doi.org/10.1017/S0263574715000090 Published online by Cambridge University Press

where:

$$\mathbf{v}_{21} \equiv \mathbf{v}_2 - \mathbf{v}_1, \quad \mathbf{v}_{31} \equiv \mathbf{v}_3 - \mathbf{v}_1 \tag{62}$$

are the so-called *kinematic generators*, which are responsible for the generation of the angular velocity vector of the mobile platform of the manipulator. Geometrically, a value of the angularity $\eta$ close to 0 means that the mobile platform has a small sensitivity to changes in rotation, whereas a value of the angularity $\eta$ close to 1 means that the mobile platform has a large sensitivity to changes in rotation.

Equations (61) and (62) show that the computation of the angularity index requires only the knowledge of the velocity vectors of any three attachment points of the mobile platform.

## 6. Axiality Index

The *operation point* (OP) of a parallel manipulator is that point on the mobile platform which is used to position the workpiece being manipulated. Intuition shows that dexterity on positioning depends on the choice of the OP. Hence, the location of the OP is important in order to describe the dexterity of a parallel manipulator to position a workpiece. The sensitivity of a parallel manipulator to position a workpiece can be measured by using the *axiality index*,[13] which is denoted by Greek symbol $\sigma$, and it is given by:

$$\sigma \equiv \cos\varphi, \quad 0 \leq \sigma \leq 1, \tag{63}$$

where:

$$\varphi = \arctan\left\{\left(\frac{1}{\delta_P}\right)\left(\frac{||\mathbf{v}_{\|}||}{\dot{\phi}}\right)\right\} \tag{64}$$

$$\mathbf{v}_{\|} = \mathbf{v}_{P/O} \cdot \mathbf{k}_0 = \mathbf{v}_1 \cdot \mathbf{k}_0 = \mathbf{v}_2 \cdot \mathbf{k}_0 = \mathbf{v}_3 \cdot \mathbf{k}_0 = \mathbf{v}_4 \cdot \mathbf{k}_0 \tag{65}$$

$$\delta_P = \sqrt{b^2 - a^2} \tag{66}$$

$$a = \left\{\mathbf{r}_{O^\star/O} - \mathbf{r}_{P/O}\right\} \cdot \mathbf{k}_0 \tag{67}$$

$$b = \sqrt{\left\{\mathbf{r}_{O^\star/O} - \mathbf{r}_{P/O}\right\} \cdot \left\{\mathbf{r}_{O^\star/O} - \mathbf{r}_{P/O}\right\}} \tag{68}$$

$$\mathbf{r}_{O^\star/O} = \left(\frac{1}{\dot{\phi}^2}\right)\left\{\boldsymbol{\omega}_{5/0} \times \left\{\mathbf{v}_1 - \boldsymbol{\omega}_{5/0} \times \mathbf{r}_{1/O}\right\}\right\} \tag{69}$$

$$\boldsymbol{\omega}_{5/0} = \dot{\phi}\,\mathbf{k}_0 \tag{70}$$

$$\mathbf{r}_{1/O} = \mathbf{r}_{P/O} + \mathbf{r}_{1/P} = (x + \rho_{1X}\cos\phi,\ \ y + \rho_{1X}\sin\phi,\ \ z)^T. \tag{71}$$

Geometrically, a value of the axiality $\sigma$ close to 0 means that the OP has a small sensitivity to changes in translation, whereas a value of the axiality $\sigma$ close to 1 means that the OP has a large sensitivity to changes in translation.

For a detailed derivation of the angularity and axiality indices, the reader is referred to ref. [13].

## 7. Computational Algorithm

The computational algorithm shown in Table II has been specially developed in order to achieve a systematic computation of the angularity and axiality indices.

It is expected that Table II serves as a systematic and quick guide to compute the angularity and axiality indices associated with the Schönflies manipulator under study.

https://doi.org/10.1017/S0263574715000090 Published online by Cambridge University Press

Table II. Computational algorithm to obtain dexterity indices.

| Computational algorithm | |
|---|---|
| Parameter(s) | Equation(s) |
| 1. Design parameters. | Given-Section 8.1 |
| 2. Input motion profiles. | Given-Section 8.2 |
| 3. Rotation angle $\phi$. | (39) |
| 4. Cartesian coordinates $x$, $y$, $z$. | (36)–(38) |
| 5. Position vectors $\mathbf{r}_{D_1/C_1}$, $\mathbf{r}_{D_2/C_2}$, $\mathbf{r}_{D_3/C_3}$, $\mathbf{r}_{D_4/C_4}$. | (41)–(44) |
| 6. Velocity vector, $\mathbf{v}_{P/O}$. | (54) |
| 7. Angular velocity $\dot{\phi}$. | (56) |
| 8. Velocities of attachment points $\mathbf{v}_{1/O}$, $\mathbf{v}_{2/O}$, $\mathbf{v}_{3/O}$, $\mathbf{v}_{4/O}$. | (57)–(60) |
| 9. Kinematic generators $\mathbf{v}_{21}$ and $\mathbf{v}_{31}$. | (62) |
| 10. **Angularity index**, $\eta$. | (61) |
| 11. Position vector, $\mathbf{r}_{1/O}$. | (71) |
| 12. Angular velocity vector, $\boldsymbol{\omega}_{5/0}$. | (70) |
| 13. Position vector, $\mathbf{r}_{O^*/O}$. | (69) |
| 14. Distance, $b$. | (68) |
| 15. Distance, $a$. | (67) |
| 16. Distance, $\delta_P$. | (66) |
| 17. Velocity vector, $\mathbf{v}_{\parallel}$. | (65) |
| 18. Angle $\varphi$. | (64) |
| 19. **Axiality index**, $\sigma$. | (63) |

## 8. Case Study

This section shows the numerical results associated with the motion capabilities for a particular design of the Schönflies parallel manipulator under study.

### *8.1. Design parameters*

For this case study, based on the construction of a computer solid model of the manipulator under analysis, it was selected the following set of design parameters:

$$
\begin{aligned}
&a_1 = a_2 = a_3 = a_4 = 113.00\,\text{mm},\\
&b_1 = b_2 = b_3 = b_4 = 40.00\,\text{mm},\\
&d_1 = d_2 = d_3 = d_4 = 103\,\text{mm},\\
&h_1 = h_2 = h_3 = h_4 = 123.00\,\text{mm},\\
&L_1 = L_2 = L_3 = L_4 = 100.00\,\text{mm},\\
&R_{1X} = 215.50\,\text{mm},\ R_{2X} = 10.10\,\text{mm},\ R_{2Y} = 167.85\,\text{mm},\\
&R_{3X} = -216.36\,\text{mm},\ R_{3Y} = 23.60\,\text{mm},\\
&R_{4X} = -9.24\,\text{mm},\ R_{4Y} = -191.44\,\text{mm},\\
&\rho_{1X} = 181.10\,\text{mm},\ \rho_{2X} = 13.25\,\text{mm},\ \rho_{2Y} = 167.85\,\text{mm},\\
&\rho_{3X} = -176.69\,\text{mm},\ \rho_{3Y} = 39.75\,\text{mm},\\
&\rho_{4X} = -17.67\,\text{mm},\ \rho_{4Y} = -159.02\,\text{mm},\\
&\alpha_2 = 353.53^\circ,\ \alpha_3 = 0.00^\circ,\ \alpha_4 = 353.53^\circ,
\end{aligned}
$$

which are symbolically shown in Figs. 2–6.

### *8.2. Input motions*

In order to study the motion capabilities of the Schönflies parallel manipulator, it is convenient to propose input motions (displacement and velocity) to be produced by the manipulator's actuators. To this end, the typical displacement and velocity profiles shown in Figs. 7–10 are used as input motions.

### *8.3. Numerical values for angle $\phi$*

Analyzing the computational algorithm shown in Table II, it may be noted that a key issue of the proposed approach is related to the computation of the numerical values of angle $\phi$. To this end, it

https://doi.org/10.1017/S0263574715000090 Published online by Cambridge University Press

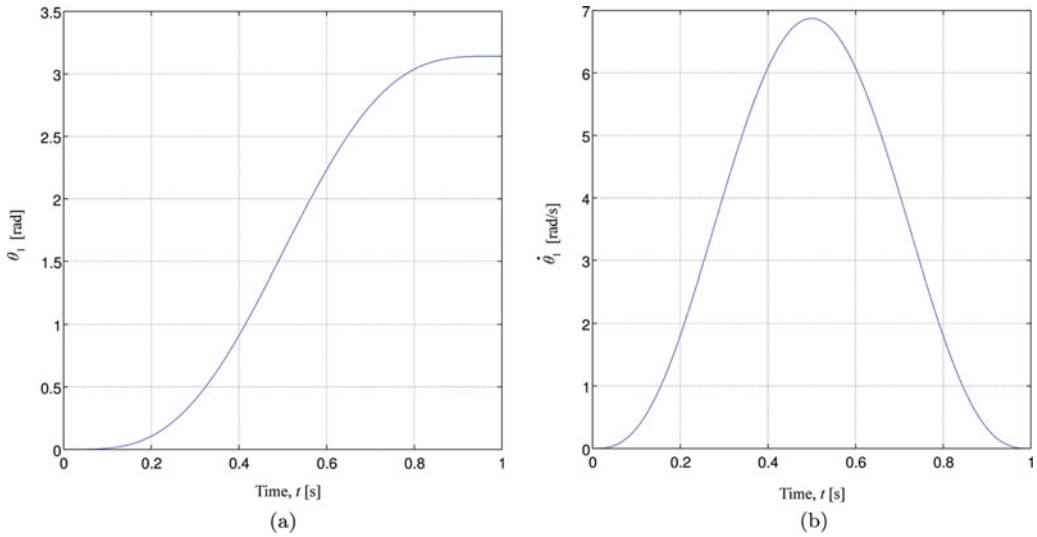


Fig. 7. Profiles for the input angle $\theta_1$: (a) displacement, and, (b) velocity.

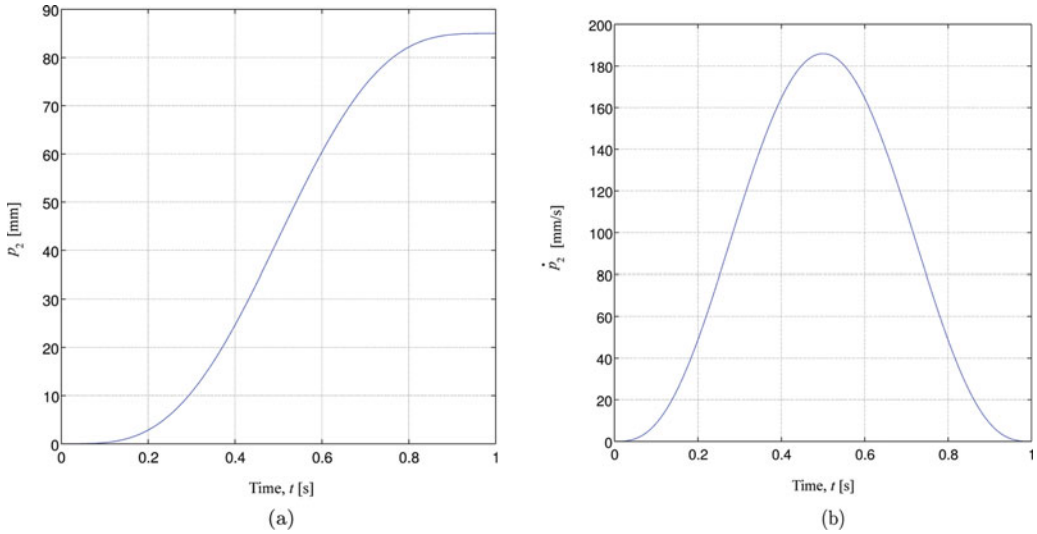


Fig. 8. Profiles for the input motion $p_2$: (a) displacement, and, (b) velocity.

should be firstly noted that Eq. (39) admits 12 solutions for parameter $\tau \equiv \tan(\phi/2)$ ($\phi = 2\arctan(\tau)$), whether real or complex, among which only the real solutions are of practical interest.

Several numerical examples were evaluated. Typically, four real solutions and eight complex solutions were obtained. From the initial real solutions ($t = t_0$), it was arbitrarily selected one, $\phi_0$, for which the manipulator could be assembled. Next, time was updated, $t = t_0 + \Delta t$, each new real solution was compared with the previous assembly solution, and the closest solution was chosen. This process was repeated for $t_0 = 0.0s \leq t \leq t_F = 1.0s$, with a step size $\Delta t = 0.0025s$. The resulting numerical values of $\phi$ were compared with those numerical results generated by means of a commercial software for the simulation of mechanical systems. This comparison is graphically illustrated by means of the plots shown in Fig. 11, where it may be observed that both plots are identical.

### *8.4. Graphical illustration of velocity patterns*

Figures 12–15 were specially conceived in order to get a complete visualization of the different velocity vectors involved into the computation of the dexterity indices. These are three dimensional drawings specially focused on the velocity patterns of points 1, 2, and 3 of the mobile platform.

https://doi.org/10.1017/S0263574715000090 Published online by Cambridge University Press

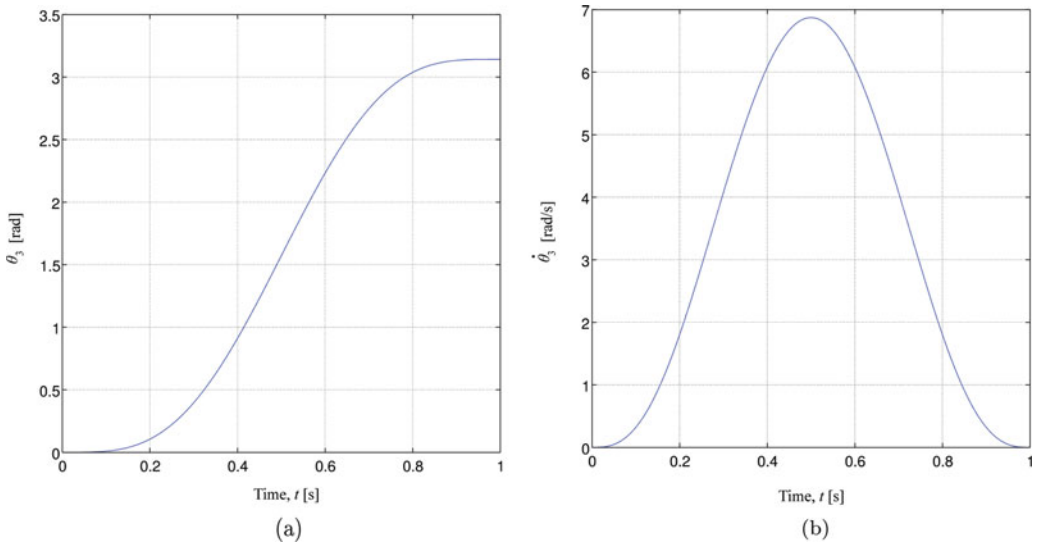


Fig. 9. Profiles for the input angle $\theta_3$: (a) displacement, and, (b) velocity.

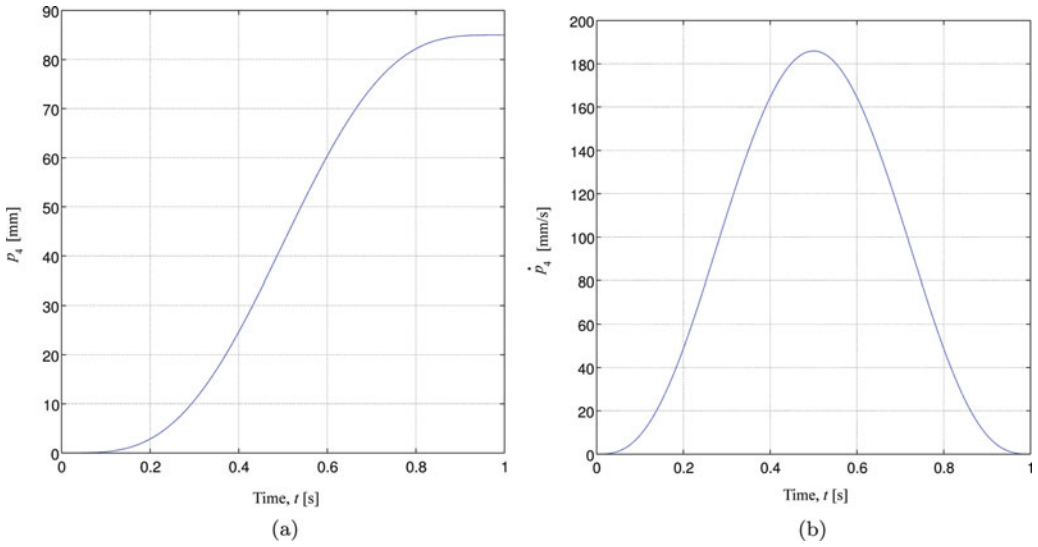


Fig. 10. Profiles for the input motion $p_4$: (a) displacement, and, (b) velocity.

On the one hand, the upper part of Figs. 12–15 shows the velocity distribution related to three chosen points in the mobile platform. Such a graphical illustration was inspired by the work presented in reference.[18]

In all these figures, it is preserved the principle of rigidity, namely, that the velocity vectors of points 1 and 2, for example, have components along the corresponding line $\mathcal{L}_{21}$ that are equal, and that all of velocity vectors of points located along line $\mathcal{L}_{21}$ have their tips distributed in a straight line array. A similar reasoning is also valid for points 1 and 3, and, 2 and 3, respectively. In this way, it is thus assured that the set of three chosen points is a velocity-consistent set.

On the other hand, the lower part of Figs. 12–15 shows the velocity vectors at three points 1, 2, and 3 in the moving platform, and also the relative orientation between the so-called *kinematic generators*, namely, $\mathbf{v}_{21}$ and $\mathbf{v}_{31}$. 2 It is important to mention that the term ISA, appearing in the lower part of Figs. 12–15, stands for *instantaneous screw axis*, see reference[19] for additional details.

Additionally, Figs. 12–15 show also that, regardless of their size, kinematic generators $\mathbf{v}_{21}$ and $\mathbf{v}_{31}$ maintain a constant angle of 29.05° between them at any configuration of the manipulator. As it will be shown later, this fact is directly related to the angularity index.

https://doi.org/10.1017/S0263574715000090 Published online by Cambridge University Press

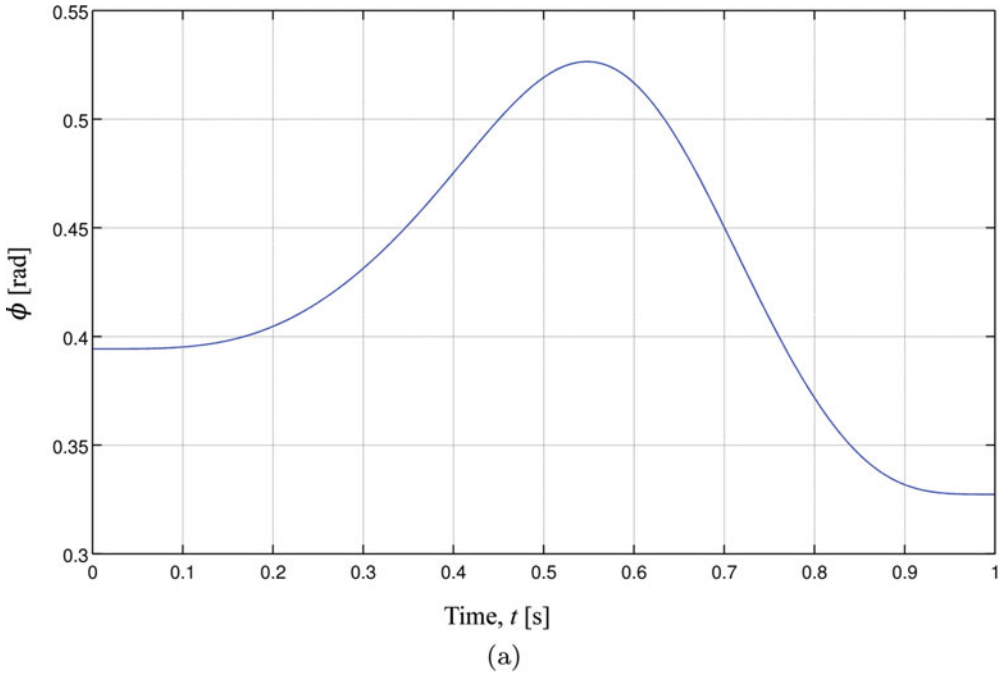


(a)

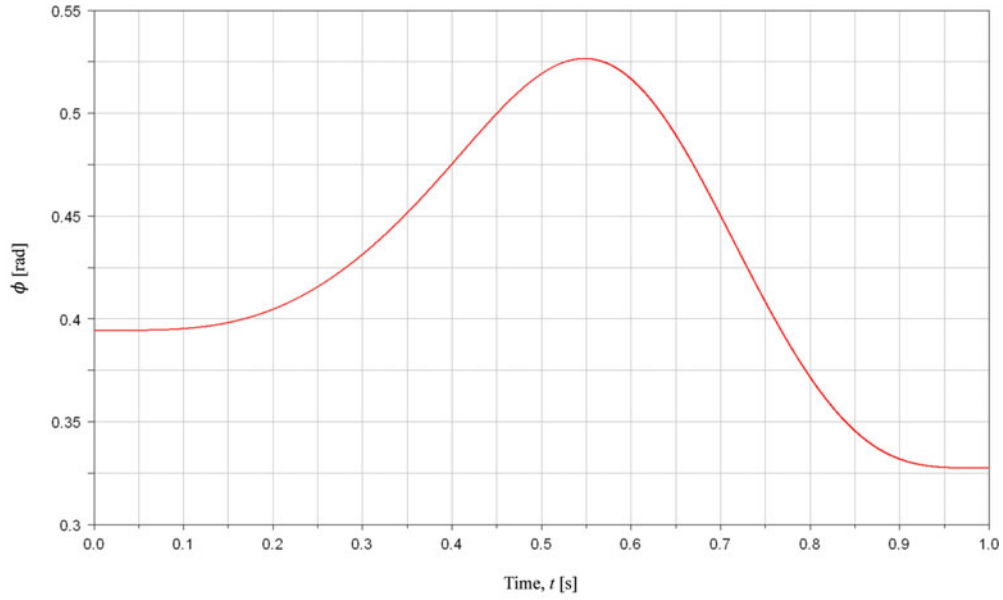


(b)

Fig. 11. Plots of angle $\phi$: (a) using Eq. (39), and, (b) using a commercial software.

### *8.5. Angularity plot*

Considering Figs. 7–10 as input motion profiles, and based on Table II, Eq. (61) was implemented in a worksheet of a commercial software package, which has symbolic computation capabilities. As a result of such implementation, there was obtained the angularity plot shown in Fig. 16.

As it is shown in Fig. 16, the angularity index maintains a constant value of $\eta = 0.4856$ for any value of parameter $t$. This is due to the fact that all the points on the mobile platform have the same velocity component along $Z_0$ axis, which agrees with the motion features associated with the Schönflies manipulator under study. In consequence, and because of their definition, namely, $\mathbf{v}_{21} \equiv \mathbf{v}_2 - \mathbf{v}_1$, and $\mathbf{v}_{31} \equiv \mathbf{v}_3 - \mathbf{v}_1$, it may be observed that kinematic generators $\mathbf{v}_{21}$ and $\mathbf{v}_{31}$ must lie on a plane containing points 1, 2, and 3 in the mobile platform. Additionally, vector $\mathbf{v}_{21}$ must be also

https://doi.org/10.1017/S0263574715000090 Published online by Cambridge University Press

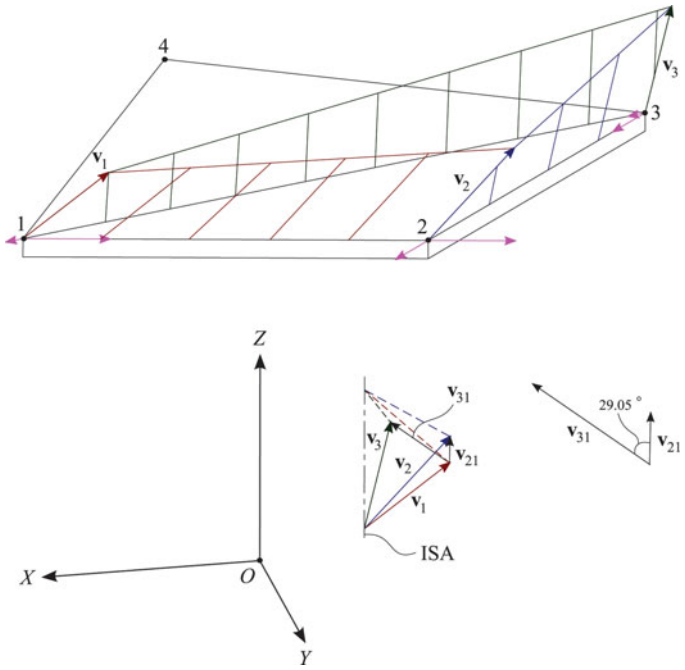


Fig. 12. Graphical illustration of velocity pattern for $t = 0.2\,\mathrm{s}$.

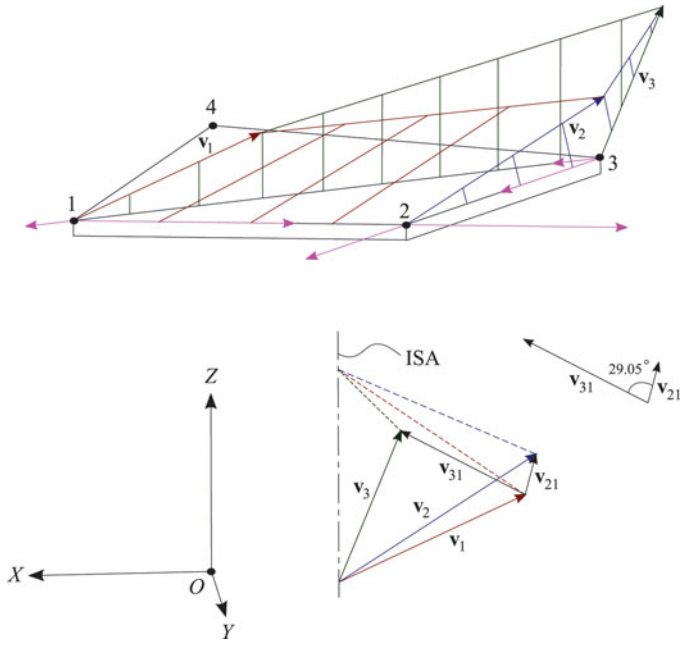


Fig. 13. Graphical illustration of velocity pattern for $t = 0.4\,\mathrm{s}$.

perpendicular to a line $\mathcal{L}_{21}$ passing through points 1 and 2, whereas vector $\mathbf{v}_{31}$ must be perpendicular to a line $\mathcal{L}_{31}$ passing through points 1 and 3.[13,19]

From the foregoing observations, it may be concluded that kinematic generators maintain a constant orientation angle between them at any configuration of the manipulator. If such angle is denoted by symbol $\gamma$, then, from Eq. (61):

$$\eta = \frac{\|\mathbf{v}_{21} \times \mathbf{v}_{31}\|}{\|\mathbf{v}_{21}\|\|\mathbf{v}_{31}\|} = \frac{\|\mathbf{v}_{21}\|\|\mathbf{v}_{31}\| \sin\gamma}{\|\mathbf{v}_{21}\|\|\mathbf{v}_{31}\|} = \sin\gamma. \tag{72}$$

https://doi.org/10.1017/S0263574715000090 Published online by Cambridge University Press

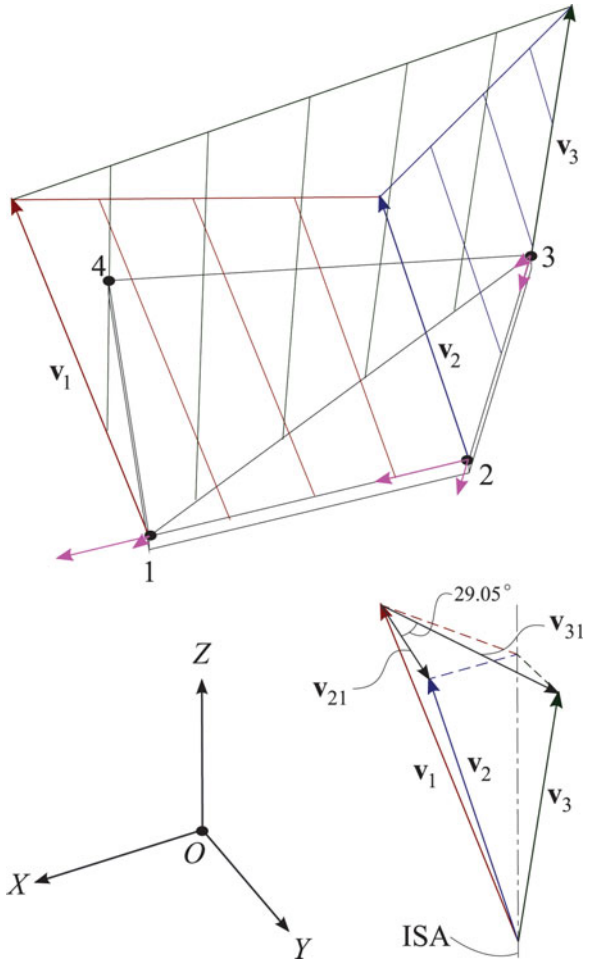


Fig. 14. Graphical illustration of velocity pattern for $t = 0.6$ s.

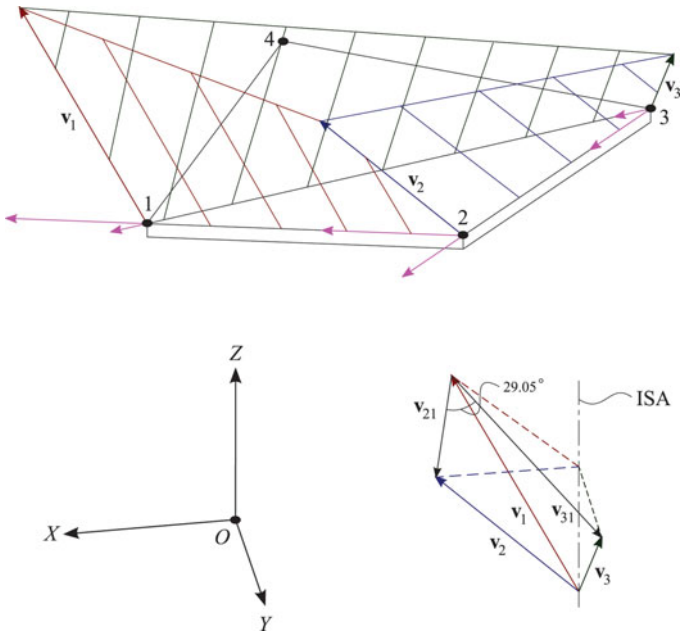


Fig. 15. Graphical illustration of velocity pattern for $t = 0.8$ s.

https://doi.org/10.1017/S0263574715000090 Published online by Cambridge University Press

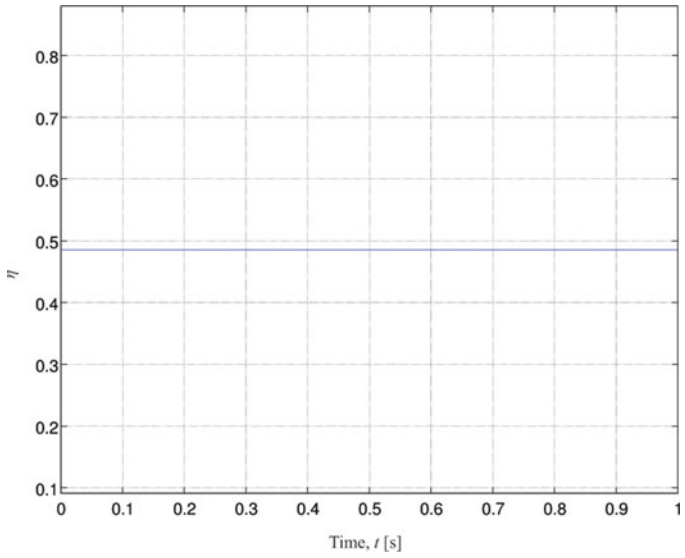


Fig. 16. Plot of the angularity index.

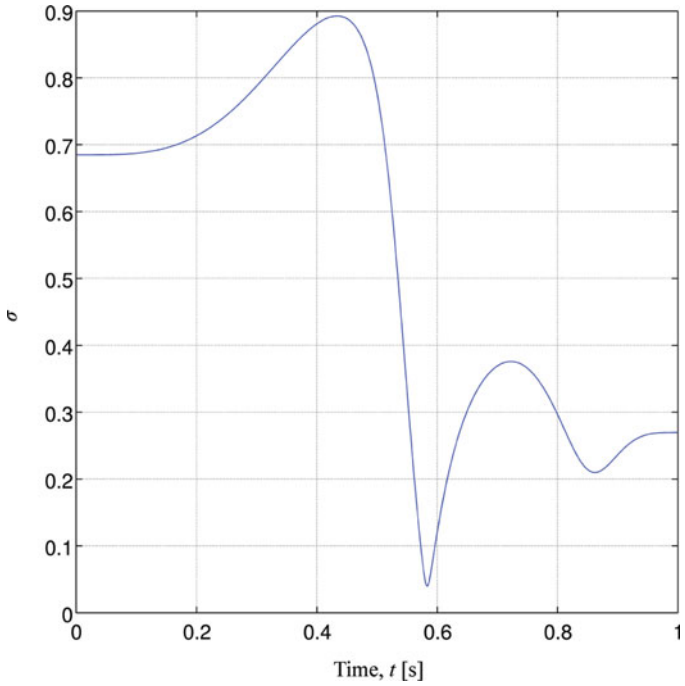


Fig. 17. Plot of the axiality index.

Furthermore, a careful observation of Figs. 12–15 reveals that $\gamma = 29.05^\circ$. Therefore, from Eq. (72), it is obtained that $\eta = \sin(29.05^\circ) = 0.4855$.

Finally, it should be observed that angle $\gamma$ is equal to the angle formed by lines $\mathcal{L}_{21}$ and $\mathcal{L}_{31}$.

### *8.6. Axiality plot*

Considering Figs. 7–10 as input motion profiles, and based on the computational algorithm shown in Table II, Eq. (63) was implemented in a worksheet of a commercial software package, which has symbolic computation capabilities. As a result, there was obtained the axiality plot shown in Fig. 17.

On the other hand, because of Fig. 17 shows a plot of the axiality of the manipulator, it may serve to measure the sensitivity of the mobile platform to changes in translation. This plot presents a maximum value $\sigma_{\text{MAX}} = 0.8924$ at $t = 0.433$ s, and a minimum value $\sigma_{\text{MIN}} = 0.03975$ at $t = 0.583$ s.

https://doi.org/10.1017/S0263574715000090 Published online by Cambridge University Press

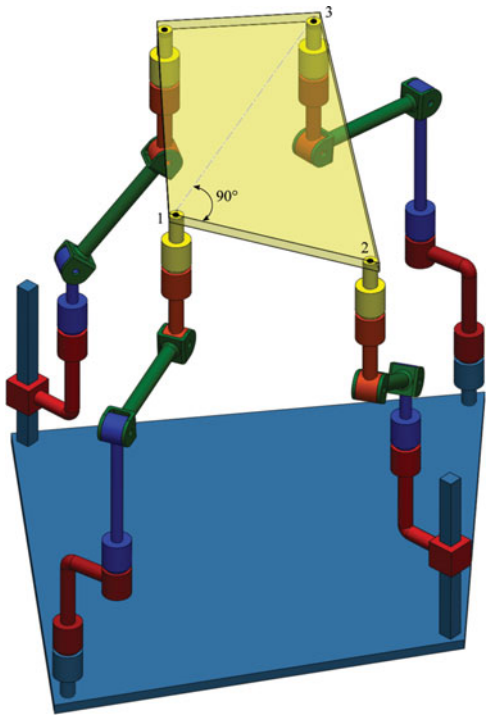


Fig. 18. Schönflies manipulator designed to produce $\eta = 1$.

This means that the best sensitivity of the mobile platform to changes in translation is achieved when time $t = 0.433$ s.

## 9. Extended Application

It was previously concluded that, for the Schönflies manipulator under study, the angle between kinematic generators $\mathbf{v}_{21}$ and $\mathbf{v}_{31}$ is equal to the angle formed by lines $\mathcal{L}_{21}$ and $\mathcal{L}_{31}$, which maintains a constant value for any configuration of the manipulator.

This conclusion motivated the idea of designing the mobile platform in such a way that line $\mathcal{L}_{21}$ be perpendicular to $\mathcal{L}_{31}$, that is, $\gamma = 90^\circ$. A computer solid model of the Schönflies manipulator with this particular design is shown in Fig. 18. The geometry of the corresponding mobile platform is given by the following dimensions:

$$\rho_{1X} = 110.36\,\text{mm},$$
$$\rho_{2X} = 94.03\,\text{mm},\ \rho_{2Y} = 139.04\,\text{mm},$$
$$\rho_{3X} = -130.47\,\text{mm},\ \rho_{3Y} = -28.28\,\text{mm},$$
$$\rho_{4X} = -73.91\,\text{mm},\ \text{and}\ \rho_{4Y} = -110.75\,\text{mm}.$$

For the special architecture of the mobile platform shown in Fig. 18, it was obtained the maximum value that angularity can reach, that is, $\eta = \sin(90^\circ) = 1.000$. This means that kinematic generators $\mathbf{v}_{21}$ and $\mathbf{v}_{31}$ are oriented in such a way that their contribution to generation of rotational motion is maximum.

On the other hand, in order to provide more design guidelines for the Schönflies manipulator under study, two additional designs are now introduced. It is important to note that each design involves different angles between lines $\mathcal{L}_{21}$ and $\mathcal{L}_{31}$. The main geometric features of each design are the following:

(1) Lines $\mathcal{L}_{21}$ and $\mathcal{L}_{31}$ form an angle $\gamma = 60^\circ$. For this special architecture of the mobile platform is computed a value of angularity $\eta = \sin(60^\circ) = 0.8660$. The dimensions of the mobile platform are: $\rho_{1X} = 118.03\,\text{mm}$, $\rho_{2X} = 40.38\,\text{mm}$, $\rho_{2Y} = 130.31\,\text{mm}$, $\rho_{3X} =$

https://doi.org/10.1017/S0263574715000090 Published online by Cambridge University Press

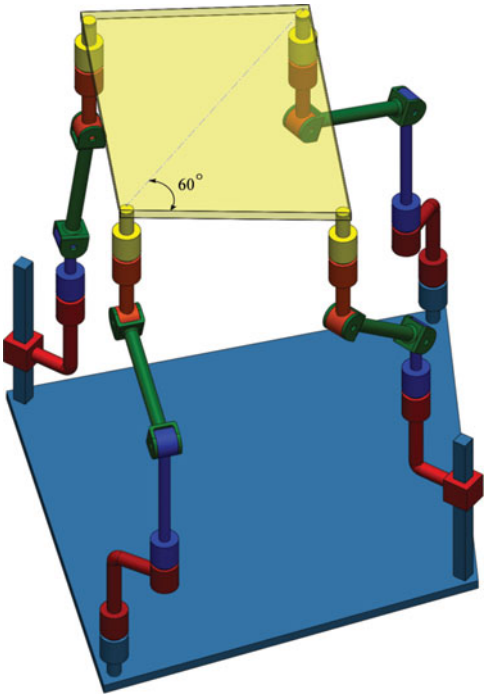


Fig. 19. Schönflies manipulator designed to produce $\eta = 0.8660$.

$-121.62\,\text{mm}$, $\rho_{3Y} = -3.30\,\text{mm}$, $\rho_{4X} = -36.78\,\text{mm}$, $\rho_{4Y} = -127.00\,\text{mm}$. A picture of this particular manipulator is shown in Fig. 19.

(2) Line $\mathcal{L}_{21}$ forms an angle $\gamma = 45^\circ$ with line $\mathcal{L}_{31}$. For this special architecture of the mobile platform is expected a value of angularity $\eta = \sin(45^\circ) = 0.7071$. The dimensions of the mobile platform are: $\rho_{1X} = 137.81\,\text{mm}$, $\rho_{2X} = 31.74\,\text{mm}$, $\rho_{2Y} = 106.06\,\text{mm}$, $\rho_{3X} = -137.81\,\text{mm}$, $\rho_{3Y} = 0.00\,\text{mm}$, $\rho_{4X} = -31.74\,\text{mm}$, $\rho_{4Y} = -106.06\,\text{mm}$. A layout of this particular manipulator is shown in Fig. 20.

Additionally, Fig. 21 shows the angularity indices for the manipulators' architectures discussed previously. It may be concluded from this figure that kinematic generators $\mathbf{v}_{21}$ and $\mathbf{v}_{31}$ are oriented in such a way that their contribution to generation of rotational motion is maximum when the angle between lines $\mathcal{L}_{21}$ and $\mathcal{L}_{31}$, namely, angle $\gamma$, is equal to $90^\circ$.

On the other hand, Fig. 22 shows the axiality profiles for the manipulators' architectures discussed previously.

It is known that the accuracy on the translational motion of a manipulator is closely related to the *axiality* index.[13] This number is to be kept close to 1, which is the maximum value that can be reached, while the smallest value that it can be attained is 0. From the foregoing discussion, Fig. 22 reveals that the axiality profile offered by the mobile platform with angle $\gamma = 90^\circ$ is better than the axiality profile associated with $\gamma = 60^\circ$. In turn, the axiality profile offered by the mobile platform with angle $\gamma = 60^\circ$ is better than the axiality profile associated with $\gamma = 45^\circ$.

### *9.1. Discussion*

On the one hand, analyzing the Jacobian matrices that appear in Eq. (45), it should be noted that both matrices, **A** and **B**, are *dimensionally inconsistent*, i.e., all their corresponding entries do not share the same units. This is because of: (a) the manipulator has a mix of revolute and prismatic actuators, and, (b) the motion of the mobile platform includes a combination of both, translational and rotational motions. In consequence, the first five indices shown in Table 1 cannot be used in the dexterity analysis of the manipulator under study.

On the other hand, based only in the dexterity indices that can be used, namely, angularity, and axiality, and taking the plots shown in Figs. 21 and 22 as evidence, it can be concluded that, from the three designs taken as examples, a mobile platform with angle $\gamma = 90^\circ$ offers the best kinematic

https://doi.org/10.1017/S0263574715000090 Published online by Cambridge University Press

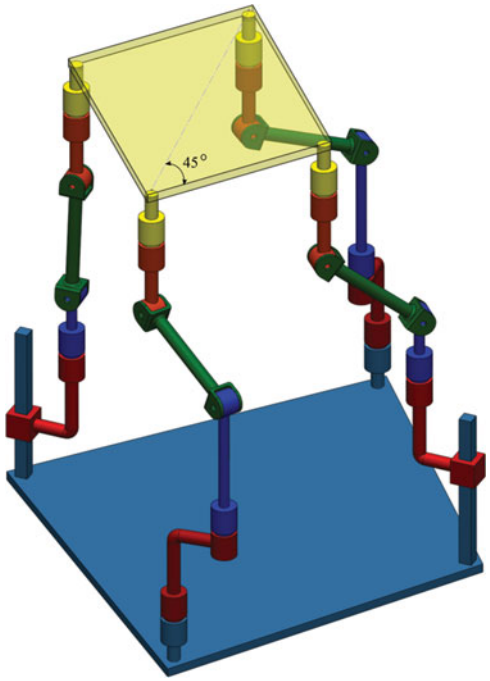


Fig. 20. Schönflies manipulator designed to produce $\eta = 0.7071$.

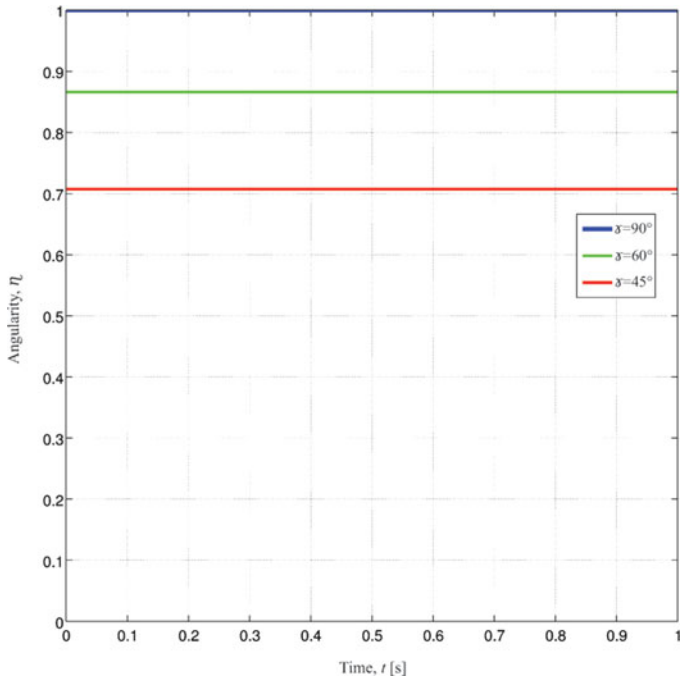


Fig. 21. Angularity plots for the Schönflies manipulators with $\gamma = 90°$, $\gamma = 60°$, and $\gamma = 45°$.

performance. Such a kinematic performance is thought in the sense of quantifying the ability of the Schönflies manipulator to position and orient its mobile platform, which is a very appreciated figure of merit for any parallel manipulator. This is because the ease of changing the position and the orientation of the mobile platform of a parallel manipulator is beneficial for design, control, and task planning purposes.

https://doi.org/10.1017/S0263574715000090 Published online by Cambridge University Press

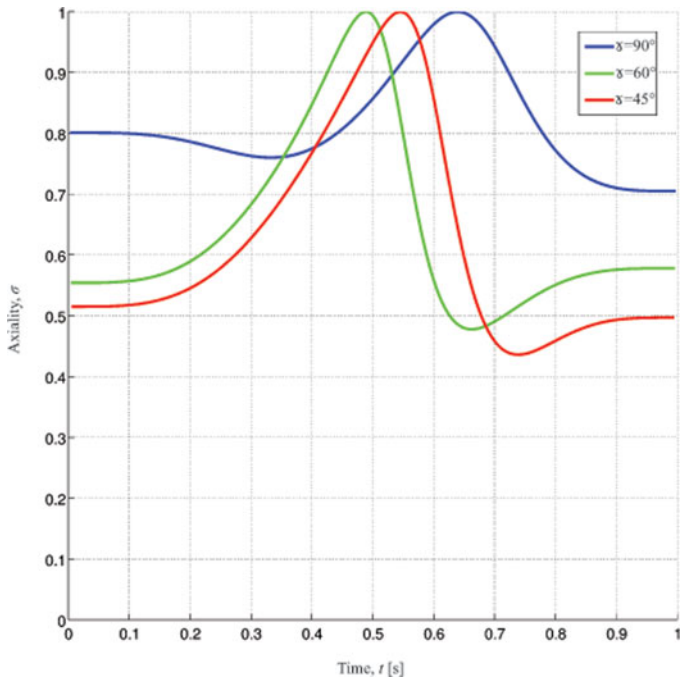


Fig. 22. Axiality plots for the Schönflies manipulators with $\gamma = 90^\circ$, $\gamma = 60^\circ$, and $\gamma = 45^\circ$.

## 10. Conclusions

Angularity and axiality indices can be used to quantify the ability of a parallel manipulator to position and orient its mobile platform, regardless of the type of actuator used. It was shown that special designs of the mobile platform may improve the kinematic performance of the Schönflies manipulator under study. This research work may serve as a guide to obtain improved designs of Schönflies parallel manipulators in the sense of achieving optimum kinematic performances, which is expected to be beneficial for design, control, and task planning purposes.

## Acknowledgments

The authors acknowledge the support of the Consejo Nacional de Ciencia y Tecnología (National Council of Science and Technology, CONACYT), of México, through SNI (National Network of Researchers) fellowships and scholarships. In addition, the financial support of the SEP-CONACYT Basic Science Project 156558 is gratefully acknowledged.

## References

1. C. M. Gosselin, "Dexterity Indices for Planar and Spatial Robotic Manipulators," *Proceedings of the IEEE International Conference on Robotics and Automation,* Cincinnati, OH, USA (1990) pp. 650–655.
2. C. A. Klein and T. A. Miklos, "Spatial Robotic Isotropy," *Int. J. Robot. Res.* **10**(4), 426–437 (1991).
3. K. H. Pittens and R. P. Podhorodeski, "A family of Stewart platforms with optimal dexterity," *J. Robot. Syst.* **10**(4), 463–479 (1993).
4. K. E. Zanganeh and J. Angeles, "Kinematic isotropy and the optimum design of parallel manipulators," *Int. J. Robot. Res.* **16**(2), 185–197 (1997).
5. T. Yoshikawa, "Manipulability of robotic mechanisms," *Int. J. Robot. Res.* **4**(2), 3–9 (1985).
6. K. Y. Tsai and K. D. Huang, "The manipulability and transmissivity of manipulators," *Int. J. Robot. Autom.* **13**(4), 132–136 (1998).
7. J. P. Merlet, "Jacobian, manipulability, condition number, and accuracy of parallel robots," *ASME J. Mech. Des.* **128**, 199–206 (2006).
8. G. Pond and J. A. Carretero, "Quantitative dexterous workspace comparison of parallel manipulators," *Mech. Mach. Theory* **42**(12), 1388–1400.
9. P. Cardou, S. Bouchard and C. Gosselin, "Kinematic-sensitivity indices for dimensionally nonhomogeneous Jacobian matrices," *IEEE Trans. Robot.* **26**(1), 166–173 (2010).

https://doi.org/10.1017/S0263574715000090 Published online by Cambridge University Press

10. S. G. Kim and J. Ryu, "New dimensionally nonhomogeneous Jacobian matrix formulation by three end-effector points for optimal design of parallel manipulators," *IEEE Trans. Robot. Autom.* **19**(4), 731–737 (2003).
11. M. Kong, Y. Zhang, Z. Du and L. Sun, "A Novel Approach to Deriving the Unit-Homogeneous Jacobian Matrices of Mechanisms," *Proceedings of the IEEE International Conference on Mechatronics and Automation*, Harbin, China (August 5–8 2007) pp. 3051–3055.
12. H. Liu, T. Huang and D. G. Chetwynd, "A method to formulate a dimensionally homogeneous Jacobian of parallel manipulators," *IEEE Trans. Robot.* **27**(1), 150–156 (2011).
13. J. Jesús Cervantes-Sánchez, J. M. Rico-Martínez and V. H. Pérez-Muñoz, "Two natural dexterity indices for parallel manipulators: Angularity and axiality," *ASME J. Mech. Robot.* **6**, Paper No. 041007 (2014).
14. G. I. Pérez-Soto, J. M. Rico, J. J. Cervantes-Sánchez, P. C. López-Custodio, L. A. Gallardo-Mosqueda and K. A. Camarillo-Gómez, "A New Method for the Kinematic Synthesis of Parallel Platforms," *Proceedings of the ASME DETC 2014*, Buffalo, N. Y., USA (August 17–20, 2014) pp. 1–14.
15. X. Kong and C. M. Gosselin, *Type Synthesis of Parallel Mechanisms* (Springer, New York, 2007) pp. 154–156.
16. L. Brand, *Vector and Tensor Analysis*, vol. 46 (John Wiley and Sons, New York, 1947).
17. J. Angeles, *Fundamentals of Robotic Mechanical Systems: Theory, Methods and Algorithms*, vol. 82 (Springer, New York, 2014).
18. J. Phillips, *Freedom in Machinery: Introducing Screw Theory*, vol. 1 (Cambridge University Press, New York, 1984) pp. 69–72.
19. J. Angeles, *Rational Kinematics* (Springer-Verlag, New York, 1989) pp. 49–50.